LOW TEMPERATURE PHOTOLUMINESCENCE STUDIES OF SHALLOW ELECTRONIC STATES IN SEMICONDUCTORS

Thesis by

Andrew Thompson Hunter

In Partial Fulfillment of the Requirements

for the Degree of

Doctor of Philosophy

California Institute of Technology

Pasadena, California

1982

(Submitted September 21, 1981)

To my parents,

Cherry and Edgar

ACKNOWLEDGEMENTS

I would like to thank Dr. T. C. McGill for his support and assistance during the course of this work. I am very grateful for the opportunity to use the resources of his laboratory during my stay at Caltech.

A very rewarding aspect of doing research in this group was the interaction with the people in it. I would like to thank Dr. Darryl Smith for answering all my questions through the years. He was always ready to drop what he was doing, and answer even the most ill-defined question in a way that would further my understanding of the topic we were discussing. I would like to thank all of the other students in the group, but especially the following: Dr. Steve Lyon for his help in starting my experiments, and for his example of careful experimentation, and thorough understanding of the equipment he was using; Dr. Ken Elliot for his at times infuriating, but always thought provoking conversations on current research topics; Dr. Gorden Mitchard for helpful conversations and his incredibly organized help in building up the laboratory; Dr. Joel Schulman for late night discussions of many topics, and for introducing me to Jazz concerts; and Reuben Collins, Dr. Murray Daw, Randy Feenstra, and Christian Mailhiot for helpful conversations about my reseach, and very interesting discussions about their own research. Finally, I would like to thank the rest of my coworkers and friends at Caltech for making the last five years a very rewarding time for me.

I would also like to thank Vere Snell for her excellent and cheerful secretarial help. Larry Begay was of great help in machining parts at a moment's notice. He had many useful suggestions on designs for equipment, and always took care to understand the instruments he was building.

I wish to acknowledge the valuable help of Dr. P. Bratt of Santa Barbara Research Center, who provided me with the HgCdTe samples, and Dr. L. H. DeVaux of Hughes Research Laboratories, who gave me a number of useful suggestions on working with HgCdTe. I would like to thank Dr. R. Hart of Texas A&M University who carried out the transmutation doping of the Si samples, and Dr. M. Young of Hughes Research Laboratories for her assistance in the transmutation doping. Finally, I gratefully acknowledge Drs. H Kimura, O. J. Marsh, and H. V. Winston of the Hughes Research Laboratories for providing me with the GaAs samples and the results of Hall effect measurements on the samples.

I would like to acknowledge the financial support of the California Institute of Technology, the Air Force Office of Scientific Research, and the Office of Naval Research.

Finally, and most importantly, I would like to thank Jenna. I am grateful for many helpful discussions on reseach topics, as well as the constant support and encouragement which helped me make it through these last few years of graduate school.

ABSTRACT

This thesis describes three experiments in which low temperature photoluminescence or selective excitation luminescence was used as a probe of shallow electronic states in three different semiconductors.

Chapter 1 serves as an introduction to the other chapters. It begins with a short review of some of the theory used to describe the electronic states studied in these experiments. After a brief mention of band theory, effective mass theory for states weakly bound to charged impurity centers is reviewed. Free excitons are briefly described, as is the binding of free excitons to impurities to form bound exciton and bound multi-exciton states. This is followed by a discussion of the interaction of the electronic states with light. Light is used both to create electron-hole pairs, and is emitted when the pairs subsequently recombine. The recombination occurs after the electrons and holes have been captured into the bound states, or have relaxed to band states near the band minima in energy. The energy and lineshape of the emitted light are characteristic of the nature of the states, and in some cases the identity of the centers involved. The chapter is closed with a summary of the results of the experiments described in the other three chapters.

Chapter 2 describes a photoluminescence study of the alloy semiconductor $Hg_{1-x}Cd_xTe$. This alloy is disordered in the sense that the cation site is randomly occupied by either the Hg or the Cd, but it retains the structural order of perfect crystals. Band-to-band, band-to-acceptor, and donor-acceptor luminescence were observed in material of $x = 0.32$ and 0.48, and bound exciton recombination luminescence was observed in material of $x = 0.48$. The band-to-band lineshape and variation in intensity with pump power are appropriate to

an electron-hole plasma with recombination proceeding without wavevector conservation. From lineshape separations, acceptor binding energies of 14.0 ± 1.0 and 15.5 ± 2.0 meV were estimated for x = 0.32 and 0.48 material, respectively. Donor binding energies were estimated to be 1.0 ± 1.0 and 4.5 ± 2.0 meV, respectively. The observation of the bound exciton recombination luminescence in x = 0.48 material is consistent with Osbourn and Smith's work indicating radiative decay for the bound exciton should dominate non-radiative, Auger decay in material with x > 0.4. Shifts in luminescence energy across the sample imply a change in composition across the sample of 0.03 cm^{-1}.

The transient decay of bound multi-exciton complex lines in the photoluminescence spectrum of Si:P is reported in Chapter 3. These measurements were made to test a shell model for the multiple particle states. This model makes some predictions about the origin of the observed lines. One of these predictions is that the m^{th} member of the β series of lines is produced when a complex with $m+1$ excitons decays to form the ground state of a complex with m excitons. The α_{m+1} line, in this model, is formed by the decay of the same complex, but into an excited state of the complex with m excitons. As a test of the model, the decays of the α lines are compared to the decays of the β lines to determine whether those transitions predicted to have common initial states decayed in an identical fashion. The results are consistent with β_2 having the same initial state as α_3. The results for β_1 and β_3 are less certain. Their decays are consistent with β_1 having the same initial state as either α_2 or α_3, and with β_3 having the same initial state as α_4. Overlap between lines, uncertainty in the decay of the boron bound exciton and the presence of unidentified background make it difficult to make conclusive line assignments. However, the results are consistent with a shell model for the states, and with more recent theoretical calculations of the level structure.

Chapter 4 describes the measurement of the excited state levels of two different shallow acceptors in bulk-grown GaAs. The technique used to make the measurements was selective excitation luminescence. In this technique, the energy difference between the laser light used for excitation and the resulting luminescence yields the acceptor excited state energy. The 1S - 2S energy differences for the two samples were measured to be 21.5 and 18.5 meV, respectively. By comparing these values to those measured by two-hole transition luminescence in high quality epitaxial GaAs, the acceptors were identified as Zn and C. The measured 1S - 2P energy differences also support the identification. These studies indicate that selective excitation luminescence can be used to study shallow impurity states in heavily doped semiconductors. In particular, selective excitation luminescence can be used to identify shallow acceptors in bulk-grown GaAs, and hence can be used as a diagnostic tool for bulk-grown samples.

Parts of this thesis have been or will be published under the following titles:

Chapter 2:

Near-band-gap photoluminescence of $Hg_{1-x}Cd_xTe$, A. T. Hunter, D. L. Smith, and T. C. McGill, Appl. Phys. Lett. **37**, 200 (1980).

Luminescence from HgCdTe alloys, A. T. Hunter, T. C. McGill, accepted for publication in J. Appl. Phys. (Sept. 1981).

Chapter 3:

Transient decay of satellite lines of bound excitons in Si:P, A. T. Hunter, S. A. Lyon, D. L. Smith, and T. C. McGill, Phys. Rev. B **20**, 2431 (1979).

Chapter 4:

Selective excitation luminescence in bulk-grown GaAs, submitted for publication in Appl. Phys. Lett.

CONTENTS

CHAPTER 1

OPTICAL STUDIES OF SHALLOW ELECTRONIC STATES IN SEMICONDUCTORS

1.1 INTRODUCTION

This thesis will discuss several experiments in which optical probes were used to study shallow electronic states in semiconductors. These states are not only very interesting quantum mechanical systems, but also have a great deal to do with the optical and electrical properties of semiconductors. The experiments were designed to further our understanding of the states with both of these motivating factors in mind. Before beginning a detailed description of the experiments, some of the electronic states that occur in a semiconductor will be reviewed in Sec. 1.2. The section will cover those states relevant to the experiments described in this thesis. Then, Sec. 1.3 will describe how these electronic states interact with light, and how this interaction is used to study the states. Finally, Sec. 1.4 will summarize each of the experiments described in the thesis, explaining why the experiments were performed, and summarizing the results from each.

1.2 BACKGROUND

1.2.1 Band theory

From a fundamental point of view the physics that determines the electronic excitations of a solid is well understood. The interactions between electrons and the other charged particles of the solid are just coulomb interactions. However, the problem is not one of writing down a Hamiltonian for the system, but of finding some meaningful way of solving a very complicated many body problem. Band theory solves the problem in an approximate sense by replacing the very complicated electron-electron interactions with a mean field, and by assuming the ions form a perfect, rigid lattice.[1] The resulting band structure is a fairly successful description of the single particle electronic excitations of this perfect crystal.

Figure 1.1 is an example of a band structure diagram. The diagram shows the energy of the single particle electronic states for the semiconductor GaAs. The valence and conduction states are separated by the band gap, a region of energies for which no states are allowed. At zero temperature, all of the states in the valence band are filled, and all of the states in the conduction band are empty. The ground state wavefunction is an antisymmetrized product of all of the single particle valence states.

The assumptions used to calculate band structure are not always justified. This thesis will investigate some of the extra excitations that are introduced to describe deviations from the predictions of band theory when the assumptions are not appropriate.

1.2.2 Consequences of the breakdown of the approximations

Most of the phenomena that are described in this thesis are a consequence of the breakdown of perfect translational symmetry. This symmetry is very important in the mathemtical derivation of band theory. The periodic array of atoms assumed in the theory can be destroyed in several ways in real crystals. One of these ways is the introduction of impurity atoms. The second example of disorder occurs in alloys of two different semiconductors, where compositional fluctuations remove the translational symmetry.

Excitons[2] are the consequence of the breakdown of the mean field approximation inherent in band theory. The lowest lying excited states in band theory are formed by replacing one of the valence band electrons by a conduction band electron. The conduction band states are derived using the same mean field as for the valence band states. However, when an electron is promoted from the valence band to the conduction band, the electron no longer sees the same potential that it saw in the valence band. Its energy is lowered by

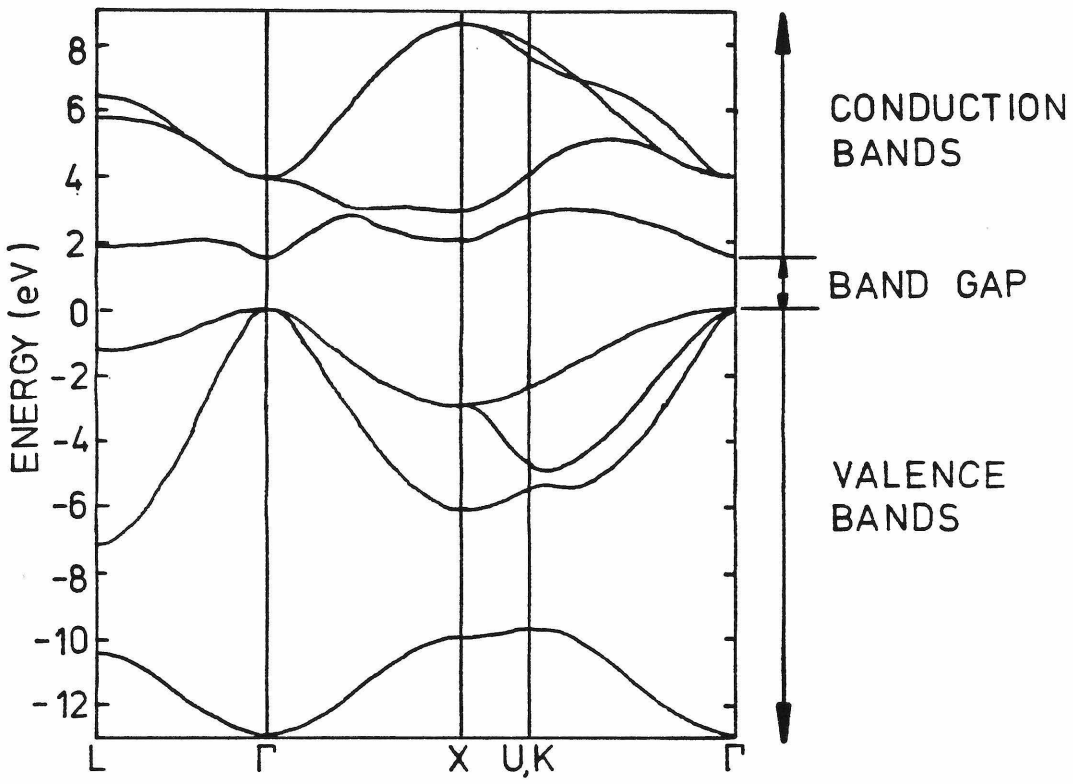

Figure 1.1: Band structure diagram of GaAs, showing electron energy as a function of electron wavevector. From J. N. Schulman, doctoral thesis, California Institute of Technology, p.42.

the interaction with the hole which is now present in the valence band. The resulting electronic states are excitons.

The effect of both the disorder and the electron-hole interaction is to introduce new states into the band gap. The introduction of states into the band gap can radically alter the properties of a semiconductor. This thesis will concentrate on electronic states formed by weak potentials, which introduce states that are near the band edges in energy. In the alloy case, this allows the problem to be approached by perturbation theory.[3] For the impurity case, and for excitons, the states are described by effective mass theory.[4]

1.2.3 Effective mass theory of impurity states

This section will review effective mass theory for electronic states bound to impurities (see Chap. 7 of Ref. 4). The new states introduced into the band gap by weak impurity potentials can be described using the electronic states derived in band theory as basis states. The form of the wavefunction for an electron on a donor or a hole on an acceptor is then

$$\Psi(\mathbf{r}) = \sum_{\mathbf{k}} A(\mathbf{k})\psi_{\mathbf{k}}(\mathbf{r}).$$

The $\psi_{\mathbf{k}}$ are electronic band states, and the $A(\mathbf{k})$ are the expansion coefficients. The sum is over the entire Brillouin zone, and all bands. In principle this sum could describe any state, no matter how strong the potential, because the band states form a complete set. However, the solution is fairly simple for potentials that are weak. The sum is substituted into the Hamiltonian for the problem and the expansion coefficients in the sum are solved for. The Hamiltonian differs from that of the ideal crystal by one term, which is $U(r) = V'(r) - V(r)$, where $V'(r)$ is the potential of an impurity atom and $V(r)$ that of a regular atom. The largest contribution to this difference is usually just a coulomb term, due to the

different charge of the ionic core of the impurity atom. For a weak and slowly varying potential $U(r)$, the solution has the following form:

$$\Psi(\mathbf{r}) \sim \varphi(\mathbf{r})\psi_{\mathbf{k}_c}(\mathbf{r}).$$

The envelope function $\varphi(\mathbf{r})$ is the fourier transform of the expansion coefficients. The electronic wave function is that of an electronic state at a critical point of the bands (either a maximum of the conduction band or a minimum of the valence band). The feature that gives the effective mass theory its name is the equation satisfied by the envelope function. The form that follows is appropriate for non-degenerate bands with extrema at $k=0$:

$$-\frac{\hbar^2}{2m_i^*}\frac{\partial^2}{\partial x_i^2}\varphi(\mathbf{r}) - \frac{e^2}{\varepsilon r}\varphi(\mathbf{r}) = E\varphi(\mathbf{r}).$$

This is very similar to the Schrodinger equation of a hydrogen atom, except that the coulomb interaction is screened by the dielectric constant(ε) of the solid, and instead of the electron reduced mass appearing in the kinetic energy term, the effective mass (m^*) of the electron appears. E is the energy of the state with respect to the band edge, $\hbar$ is Planck's constant, and e is the electronic charge. The effective mass is related to the curvature of the band at the critical point, and is defined by the equation

$$\frac{1}{m_i^*} = \frac{1}{\hbar^2}\frac{\partial^2 E(\mathbf{k})}{\partial k_i^2}.$$

Here $E(\mathbf{k})$ is the energy of the in-band electronic states.

The simplest excitations described by this theory are donor and acceptor states. A donor is produced when an atom with an extra valence electron is introduced in the solid. After forming chemical bonds with its neighbors, the

extra electron can be easily removed from the atom, leaving a positively charged center, and an electron in the conduction band. Effective mass theory describes the lowering of the energy of this electron when it is bound to the impurity. An acceptor, on the other hand, is formed when an atom deficient one valence electron is introduced into the crystal. To make up its complement of chemical bonds, it pulls an electron out of the filled valence band of the crystal, leaving a positivily charged hole in the valence band. Effective mass theory now describes the energy of the hole when it is bound to the impurity center.

For the simple non-degenerate bands mentioned above, and with the additional assumption that the effective mass is isotropic, the energy spectrum of an electron on a donor or a hole on an acceptor may be described by

$$E_n = -\frac{m^* e^4}{2\hbar^2 \varepsilon^2 n^2}.$$

where m^* is the effective mass of either the electron or the hole and n is the principal quantum number of the state. For more complex band structure, the energy spectrum is more complicated, but the results are qualitatively similar.[4,5]

Usually only the coulombic part of the impurity potential is included in the effective mass Hamiltonian. This means that all singly charged donors have the same binding energy in this model, and similarly for the acceptors. The non-coulomb part of the impurity potential is capable of changing this energy spectrum, however. This "central cell shift" can be measured in a variety of experiments. For many impurities the binding energy of the electrons or holes is characteristic of the impurity. This allows a very important application of the optical study of semiconductors, which is the identification of impurities in the crystal.

1.2.4 Bound excitons

For semiconductors of sufficiently large dielectric constant, the electron-hole interaction can be considered to be a weak potential, and an effective mass equation can be derived for the exciton.[4] The energy spectrum is given by:

$$E_n = E_g + \frac{1}{(m_e^* + m_h^*)} \frac{\hbar^2 K^2}{2} - \left(\frac{m_e^* m_h^*}{m_e^* + m_h^*} \right) \frac{e^4}{2\hbar^2 \varepsilon^2 n^2}.$$

The first term is the band gap energy. The second term is the kinetic energy of center of mass motion of the exciton. K is the wavevector of the center of mass motion, and m_e^* and m_h^* are the effective masses of the electron and hole, respectively. The final term represents the internal energy of the exciton. The exciton can be pictured as an electron bound to a hole propagating through the crystal.

The exciton, once formed, can be captured by a neutral donor or acceptor. The resulting multiple particle state is called a bound exciton.[6] There are two electons and one hole bound to a positively charged center in the donor case. The complex is the same for the acceptors, except that the charges on all the particles are reversed. The complex so formed can continue to bind more and more excitons, to produce large, many particle states, known as bound multiexciton complexes.[7,8]

1.3 RELEVANT OPTICAL PROCESSES

The experimental study of the excitations described above depends on their coupling to light. In a photoluminescence experiment, light is used to create electron-hole pairs, and light emitted as the pairs recombine is analyzed to obtain information about the electronic states occupied by the carriers before the recombination.

1.3.1 Above-band-gap absorption

Absorption of above band gap light produces excited electrons and holes. Both HgCdTe and GaAs, two of the semiconductors studied for this thesis, absorb very strongly at the photon energy of the lasers used for the excitation. This is because these materials are direct, and wavevector conserving absorption can occur. This is illustrated in the top half of Fig. 1.2, where the absorption process is drawn as a vertical transition, since the wavevector of the photon is negligible on this scale. The absorption depth for 2 eV light (approximately the energy of the lasers used for excitation) is $\sim 0.3\ \mu m$ in GaAs,[9] and probably the same order of magnitude in HgCdTe (data are given for HgTe and CdTe in Ref. 9). This absorption depth is many lattice spacings, so bulk properties are studied in the experiment.

The absorption is not as strong for the other semiconductor studied in this thesis. Si is an indirect semiconductor, which means that the conduction band minimum is not at the same point in wavevector space as the valence band maximum. Therefore, for absorption just above the band gap, a phonon must participate to conserve wavevector in the transition. This is illustrated in the bottom half of Fig. 1.2, where the nearly horizontal line represents the emission of a phonon. This is a second order process, and is much weaker than the direct absoption described above. The laser photon energy used for the Si work was ~ 1.5 eV, and is absorbed with the emission of a phonon. The absorption depth for light of this energy is $\sim 50\ \mu m$[10] so again, bulk excitations are created and studied in the experiment.

The electrons and holes very quickly lose energy by emission of optical and acoustic phonons and relax to the conduction band minimum or valence band maximum. This process occurs within nanoseconds of excitation.[11] Since

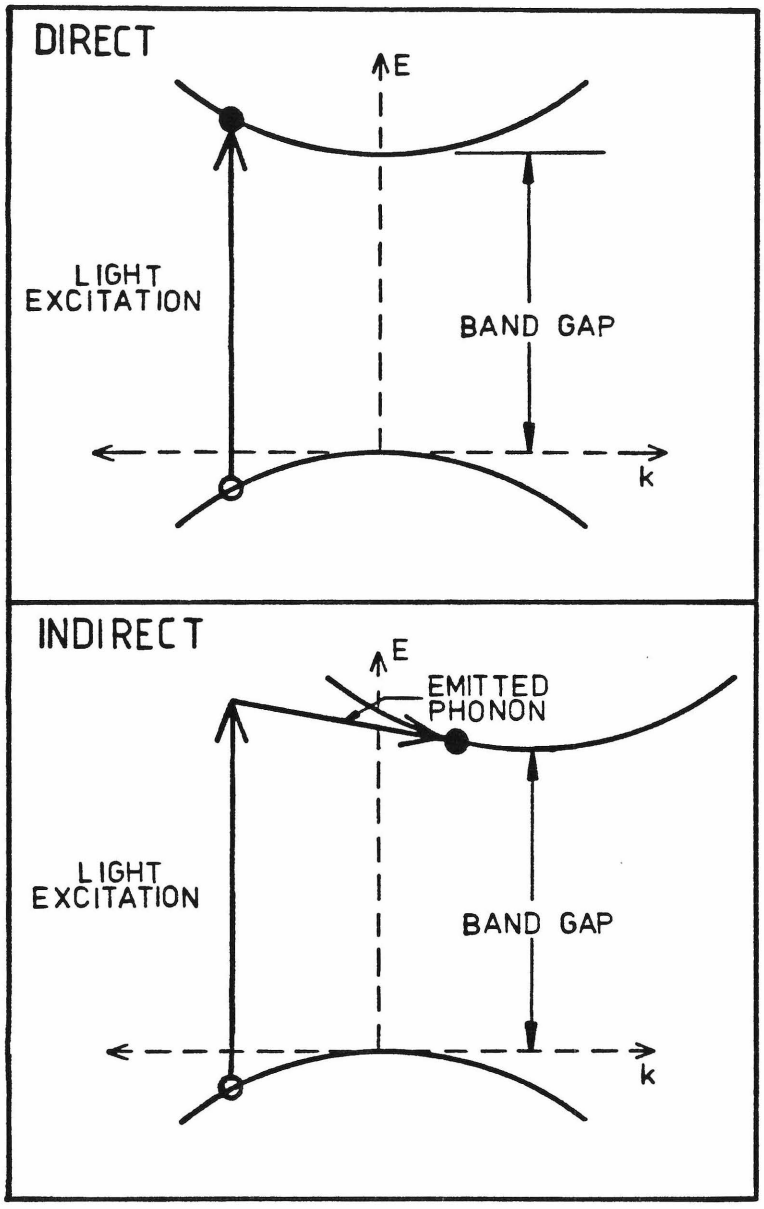

Figure 1.2: The top half of the figure is a schematic of above band gap light absorption in a direct semiconductor; the bottom half, in an indirect semiconductor.

most of the recombination processes take much longer than nanoseconds to occur, it will be assumed that the electrons and holes occupy the lowest energy states available to them, weighted by a thermal occupation probability, before recombination.

1.3.2 Luminescence processes

Recombination of electrons and holes in any of the states mentioned in the preceding sections can lead to the production of a photon. These processes are reviewed in Ref. 9, but those of importance in the interpretation of the luminescence experiments described in this thesis will be discussed briefly below.

Band-to-band recombination can take place if the temperature is sufficiently high or the exciton binding energy sufficiently low that a substantial number of carriers are not bound together as excitons. Otherwise, excitons form and the recombination energy is slightly below the band gap energy.[12,13] In both cases, wavevector conservation is expected in pure crystals.

If impurities are present, there are many other mechanisms available for recombination. Figure 1.3 is a photoluminescence spectrum of epitaxial GaAs that shows some of the possible luminescence bands. The sharp lines at 1512 and 1514 meV are acceptor and donor bound exciton lines,[6] respectively. Bound multi-exciton lines are not observed in this material, but are observed in Si[7,8,14] and in other semiconductors.[15,16] When recombination occurs in a multi-exciton complex, the energy of recombination depends on the number of excitons that are bound to the impurity. Hence, a whole series of lines is observed. In indirect material, such as Si, the bound exciton recombination can occur with the creation of a wavevector conserving phonon, but can also occur without the phonon. This no-phonon transition can take place because the bound exciton wavefunction is not localized in wavevector space, which allows a

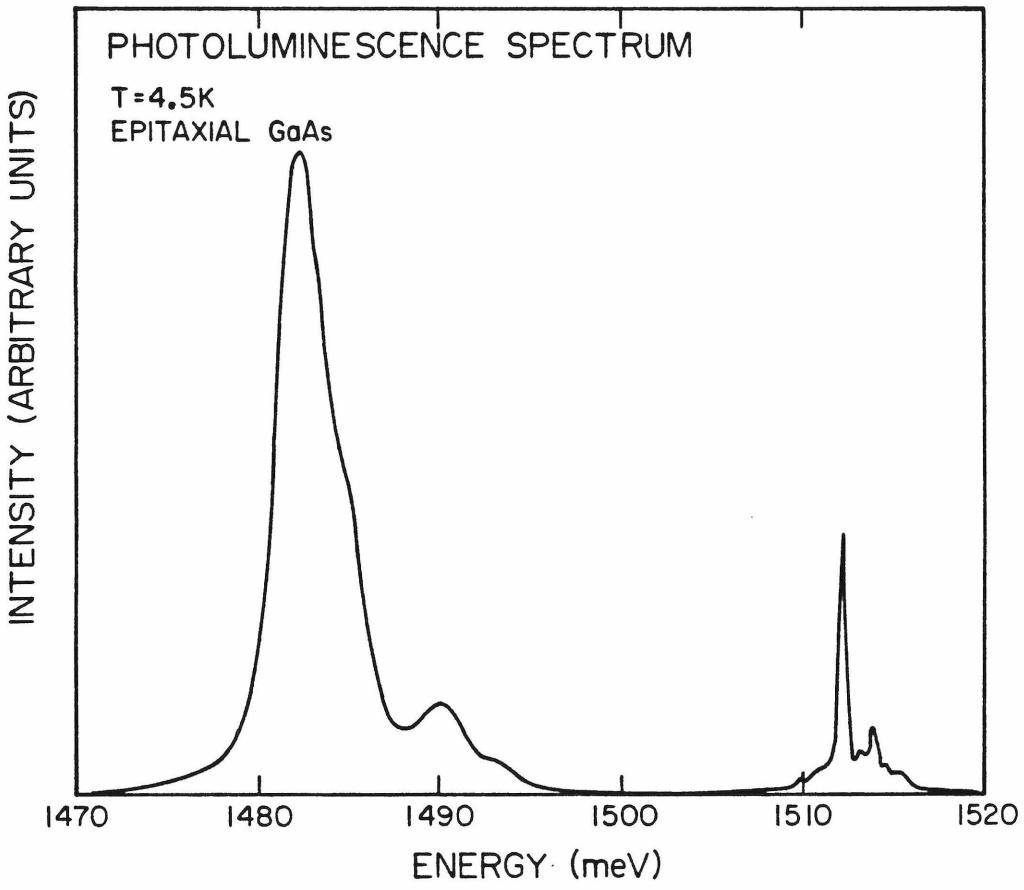

Figure 1.3: Photoluminescence spectrum of epitaxial GaAs with above band gap excitation. Intensity of emitted light is plotted against photon energy. The spectrum shows donor and acceptor bound exciton , donor-acceptor, and free electron to bound hole recombination luminescence.

small but finite overlap between the initial and final state wavevectors. It is comparable in intensity to the phonon-assisted transitions because the phonon assisted transitions are second order processes which are also weak.

The broader line at 1482 meV in Fig. 1.3 is an example of donor-acceptor luminescence,[17,18,19] in which a hole on an acceptor recombines with an electron on an adjacent donor leaving two ionized impurities in the final state. The energy of the final state is lowered by the coulomb interaction between these impurities. Since the coulomb interaction energy depends on the pair separation, a broad line is produced by this process. The high energy shoulder of this line is an example of band-to-impurity recombination luminescence.[20] In this sample, the line is caused by free electrons recombining with holes bound to a shallow acceptor. The line at 1490 meV is another donor-acceptor line, but the acceptor is different for this line than for the more intense line at lower energy. The shoulder on the high energy side of the 1490 meV line is a band-to-acceptor line associated with this second acceptor.

The radiative recombination mechanisms described above account for the luminescence spectra that will be presented in this thesis. However, there are other mechanisms that have an effect on the luminescence spectra, mostly by lowering the luminescence intensity. Non-radiative processes can directly compete with the recombination luminescence process. An example of this is Auger recombination of bound excitons and multi-excitons, in which the recombination energy is taken up by the ejection of one of the remaining particles.[21] Another competing process is recombination via deep levels, which is either non-radiative, or produces photons with energy too low to appear in the near band gap luminescence spectra.

1.3.3 Below-band-gap absorption

In a luminescence experiment in which above band gap excitation is used, the probability of occupation of a given state depends on many factors, such as the temperature and the presence of other impurity related states in the sample. The occupation does not depend in a detailed manner on the way the sample is excited. The use of tunable, below band gap laser sources allows the system to be excited into a specific state. Different information can be gained from a luminescence experiment with this source than in one with above band gap excitation.

With the absorption of below band gap light of the appropriate photon energy, the inverse of any of the luminescence processes described above can be made to occur. This will selectively populate those states that are formed by the absorption of that energy. This is particularly useful in the study of excited levels of impurity states. The energy difference between the laser and the emitted light will give the energy difference between the ground and excited levels of the impurity. This technique can also improve the intensity of luminescence signal, since a given radiative channel can be favored by the selective excitation.

1.4 SUMMARY OF THESIS

This thesis describes three different experimental projects in which the optical processes above were used as probes of electronic states in various semiconductors. The projects were a luminescence study of HgCdTe, lifetime measurements of bound multi-exciton complexes in Si, and a selective excitation luminescence experiment in GaAs to measure the acceptor excited state energies.

1.4.1 Luminescence from HgCdTe alloys

The motivation for this work was two-fold. First, this alloy semiconductor is technologically interesting. The band gap is a nearly linear function of the composition, and can range from zero (the band gap of HgTe) to 1.6 eV (the band gap of CdTe at zero temperature).[9] Therefore, an intrinsic infrared detector can be made from this material whose response is tailored to whatever wavelength range is of interest. The second reason for studying the material is that it is disordered. While truly amorphous materials prove to be very difficult to analyze theoretically, the alloy material still has the structural order of perfect crystalline material, and some of the techniques appropriate to a perfect crystal can still be applied. Insight into the effects of disorder can be gained by investigating departures from the perfect crystal results. The experiments were done not only to gain any information possible on HgCdTe, but more specifically to check some of the theoretical work being done at the same time by other workers in our group concerning the electronic states in HgCdTe.

The principal results of this project are as follows. First, a luminescence line due to bound exciton recombination was observed, for the first time in HgCdTe. The presence of this line in material with x = 0.48 (x is the fraction of CdTe) was consistent with the calculation by Osbourn and Smith[21] which predicted radiative decay of bound excitons should dominate non-radiative, Auger decay of bound excitons in material with more than 40% CdTe. The line was not observed in material with x = 0.32. The width of the bound exciton line is a measure of the disorder of the crystal within a bound exciton Bohr radius of the impurity, and the width measured is consistent with the theoretical value calculated by Smith.[22]

The band-to-band line was appropriate to an electron-hole plasma with

recombination proceeding without wavevector conservation. In a semiconductor which is not an alloy, this type of recombination is very unlikely, except under conditions of very high impurity or free carrier concentrations.[23] In the alloy, the wavevector selection rule is relaxed by the inherent lack of translational symmetry caused by compositional fluctuations.

Donor-acceptor and free electron to bound hole luminescence bands were also observed. The position of these bands allowed estimates of the donor and acceptor binding energies to be made.

Finally, shifts in composition across the samples were measured by the shift in energy of the luminescence bands as the pump laser was scanned across the sample. In this case it is large scale fluctuations in composition that are being measured.

1.4.2 Lifetime measurements in Si

The lifetime measurements of bound multi-exciton complexes in silicon were motivated by lively theoretical interest in the origin of these lines. A shell model[24] of the multi-particle states had been proposed. This model predicted that certain of the luminescence lines observed were caused by transitions starting from the same initial state. The decay of the luminescence should be identical for each line, if the lines are due to transitions which originate on the same level. This prediction was checked by measuring the intensity of the luminescence of appropriate lines as a function of time after excitation stopped.

These measurements indicated that the decay of the lines was consistent with the predictions of the shell model. While this was not positive evidence for the model, it did eliminate a very decisive negative test. Careful account of the overlap between lines was made in the analysis of the decays.

This overlap changed the apparent decay times of some of the lines, and it proved to be necessary to follow the decays over three or four orders of magnitude in intensity to obtain a reliable estimate of the effect of this overlap.

In order to make measurements of the required accuracy, a transient recording system was constructed. This system timed the arrival of each photon with respect to the excitation laser pulse. The data were stored in a digital manner, which allowed the use of a computer in the analysis of the decays.

1.4.3 Selective excitation luminescence in GaAs

This work was done primarily to investigate methods for studying impurity states in bulk grown GaAs. A knowledge of the excited state spectrum of acceptor levels could be used to identify impurities. The problem was to measure the spectrum in the bulk-grown material, where methods used in less heavily doped epitaxially grown GaAs were not as useful. A method was used for the first time in GaAs utilizing a tunable dye laser to determine the ground to excited state energy spacings of the acceptors in bulk grown GaAs.

The excited state spectra of the principal acceptors in two different GaAs samples were measured. The technique, called selective excitation luminescence, used a tunable dye laser to selectively populate donor-acceptor pairs with the acceptor in an excited state. The holes quickly relaxed to their ground states, where they recombined with the electrons, emitting photons. The energy difference between the laser light and the luminescence was the energy difference between the ground and excited state of the acceptor. The ground to excited state energy difference reflects the central cell shift of the ground state energy, and is a signature of the particular impurity. Using values measured for the energy differences by different methods in epitaxial GaAs, the acceptors were conclusively identified in the bulk grown samples, where these other methods

are not useful.

REFERENCES

1. O. Madelung, *Introduction to Solid-State Theory*, (Springer-Verlag, Berlin, 1978).

2. R. S. Knox, *Theory of Excitons* (Academic Press, New York, 1963).

3. R. H. Parmenter, Phys. Rev. **97**, 587 (1955).

4. F. Bassani, G. P. Parravicini, *Electronic States and Optical Transitions in Solids* (Pergamon, Oxford, 1975).

5. See, for example, A. Baldereschi, and N. O. Lipari, Phys. Rev. B **8**, 2697 (1973).

6. J. R. Haynes, Phys. Rev. Lett. **4**, 361 (1960).

7. A. S. Kaminskii, Y. E. Pokrovskii. amd N. V. Alkeev, Zh. E. T. F. **59**, 1937 (1970).

8. R. Sauer, Phys. Rev. Lett. **31**, 376 (1973).

9. J. I. Pankove, *Optical Processes in Semiconductors*, (Dover, New York, 1971).

10. S. M. Sze, *Physics of Semiconductor Devices*, (Wiley, Interscience, New York, 1969) p. 54.

11. J. C. Hensel, and K. Suzuki, Phys. Rev. B **9**, 4219 (1974).

12. R. J. Elliot, Phys. Rev. **108**, 1384 (1957).

13. R. B. Hammond, D. L. Smith, and T. C. McGill, Phys. Rev. Lett. **35**, 1535 (1975).

14. K. Kosai, and M. Gershenzon, Phys. Rev. B **9**, 723 (1974).

15. P. J. Dean, D. Herbert, D. Bimberg, and W. J. Choyke, Phys. Rev. Lett. **37**, 1635 (1976).

16. R. W. Martin, Solid State Commun. **14**, 369 (1974).

17. J. J. Hopfield, D. G. Thomas, and M. Gershenzon, Phys. Rev. Lett. **10**, 162 (1963).

18. D. J. Thomas, J. J. Hopfield, and W. M. Augustyniak, Phys. Rev. **140**, A202 (1965).

19. M. R. Lorentz, T. N. Morgan, and A. P. Pettet, in Proceedings on the Physics of Semiconductors, edited by S. M. Ryvkin (Nauka, Leningrad, 1968), p. 495.

20. D. M. Eagles, J. Phys. Chem. Solids **16**, 76 (1960).

21. G. C. Osbourn, and D. L. Smith, Phys. Rev. B **20**, 1556 (1979).

22. D. L. Smith, unpublished.

23. G. Lasher, and F. Stern, Phys. Rev. **133**, A553 (1964).

24. G. Kirczenow, Can. J. Phys. **55**, 1787 (1977).

CHAPTER 2

LUMINESCENCE FROM HgCdTe ALLOYS

2.1 INTRODUCTION

2.1.1 Motivation for work

$Hg_{1-x}Cd_xTe$ is an example of a crystalline alloy semiconductor.[1] This material has a zincblende crystal structure, which is characterized by the superposition of two face centered cubic sub-lattices. One sub-lattice has an anion (Te, in this material) on each lattice point. The other sublattice is displaced from the first by (1/4,1/4,1/4)a, where a is the length of the cube edge. This sublattice has a cation on each lattice point. In an ideal alloy, the probability is x that the cation on a particular site is Cd, and 1-x that the cation is Hg.

These alloy systems are very interesting from a theoretical point of view, as they are examples of systems with an intermediate amount of disorder. Many of the theoretical techniques developed to deal with semiconductors make use of the perfect periodicity of the lattice. Structurally disordered systems, such as amorphous semiconductors, are therefore very difficult to deal with theoretically because they lack this long range order. Crystalline alloys are somewhere in between perfect crystals and amorphous materials, and can be investigated without abandoning all of the theoretical techniques developed for the perfect crystalline case. Thus, studies of these systems can provide insight into the effects of disorder.

The alloy systems have interesting and practical applications.[1] Since the band gap can be adjusted by varying the relative concentration of the alloy components, detectors can be constructed with their response tuned for some particular range of photon energies. In the case of HgCdTe the band gap can be varied from -0.3 (the zero temperature band gap of HgTe)[2] to 1.6 eV (the zero temperature band gap of CdTe)[2]. This allows the construction of intrinsic HgCdTe detectors with their response tailored to regions of the infrared with

atmospheric absorption windows. Consequently, these studies are also motivated by a need to better understand the physics of the material as an aid to predicting device performance.

Luminescence experiments can yield important information about the properties of HgCdTe; however, few experiments[3,4] of this type have been reported in the literature. Therefore, we have carried out a series of photoluminescence experiments as a probe of the near band gap electronic states of the material, and of transitions between these states.

2.1.2 Relevant theoretical calculations

The virtual crystal approximation[5,6] is one technique developed for dealing with crystalline alloys. The random part of the crystal potential is separated from the rest of the potential and treated as a perturbation. The periodic part is constructed by placing a weighted average of the anion potentials on each anion site, instead of the actual anion potential which depends on which species occupies the site.[6] Many of the properties of the semiconductor can be predicted by basing calculations on this "virtual" periodic crystal. Thus, to lowest order, the alloy will be treated as a perfect crystal, with all the calculated parameters a function of the composition, x. This by itself is an interesting feature of alloy systems, since the functional dependence can be tested experimentally by examining a variety of compositions.

A specific example of this type of calculation relevant to our experiments is a calculation by Osbourn and Smith[7] pertaining to the lifetime of bound-excitons in HgCdTe. They calculate the decay rate of bound excitons by both radiative decay and non-radiative Auger decay as a function of composition, in the virtual crystal approximation. Their calculation suggests radiative decay of bound excitons should dominate Auger decay in HgCdTe material with

CdTe concentration of over 40%.

The virtual crystal approximation ignores the effects of disorder. However, disorder may be included by treating the difference between the real and virtual crystal potentials in perturbation theory.[6] The calculation in Ref. 6 showed that while the disorder had no first order effect on the energy of the electrons, in second order it caused a shifting of states into the band gap. Perturbation theory that begins with the virtual crystal states cannot describe the limiting case of bound state, however.[6] Bound states can be added to the description by starting with the zero order virtual crystal states, then treating concentration fluctuations as local potentials. These potentials are able to trap the free carriers into bound states with energy in the band gap.[8,9] Both of these approaches predict a finite density of states in the band gap,[6,8,9] which can result in low energy tails on luminescence or absorption processes. Even for more energetic carriers not actually in these in-gap states, the fluctuations can act as additional scattering centers.[10] This scattering can also cause substantial changes in the luminescence spectra from the results expected for a perfect crystal.

The disorder also has an effect on the bound states formed by impurities. The width of various bound levels due to the compositional fluctuations have been calculated[11] The mean composition in the small volume occupied by the bound electron or hole can differ from the mean value in the crystal as a whole. Since the binding energy of the carrier depends on the composition, the width of the level will be inhomogeneously broadened by the fluctuations in composition.

There are other more recent methods for treating disordered systems than the virtual crystal approximation.[1,12,13] However, since the virtual crystal

approximation adequately accounts for the data presented here, we will not consider these other models except to note that they exist, and may treat the disorder in a more realistic fashion.[1,12]

2.1.3 Previous experimental results

Previous experimental work on HgCdTe of relevance here does include a small amount of both photoluminescence[3,4] and cathodoluminescence.[4] Two broad luminescence bands were observed, which were attributed to band-to-band and band-to-impurity transitions.[3,4] The impurity was thought to be Hg-vacancies.[4] However, acceptor ionization energies estimated from luminescence did not agree with Hall effect measurements.[3] Temperature dependence of Hall measurements for x = 0.32 material indicated an acceptor with an activation energy of about 20 meV, but luminescence line separations gave acceptor ionization energies of 25 meV in the x = 0.5 material, and as low as 10 meV in x ~ 0.3 material.[3] Another group has done some additional Hall work, taking compensation into account, and checked their resulting acceptor energies by performing far infrared photoconductivity experiments.[14] These measurements yield an acceptor binding energy E_A=14.0± 1.0meV for material with x = 0.4.[14]

2.1.4 Results of this work

In these experiments, band-to-band, band-to-acceptor and donor-to-acceptor, and bound exciton recombination luminescence were observed. The experiments were performed on samples of x = 0.32 and 0.48, for temperatures less than 30 K, and for excitation densities between 0.3 and 14.0 W cm^{-2}. Three samples of x = 0.48 material were studied, two p-type and one n-type, and two samples of x = 0.32 material were studied, both p-type.

The analysis of these luminescence lines provided information about the important physical processes occurring in, and characteristics of, the

HgCdTe samples. The lineshape and shift with temperature of the band-to-band line indicated that the recombination was proceeding without wavevector conservation, providing information on fluctuation scattering of free carriers. An analysis of the donor-to-acceptor and band-to-acceptor luminescence lines gave donor and acceptor binding energies. The observation of the bound exciton luminescence provided a check on the lifetime calculation done by Osbourn and Smith.[7] Finally, the luminescence experiments provided other useful information on the HgCdTe samples that were measured, such as the presence of compensating centers, macroscopic composition changes across the sample, and laser power-density damage thresholds.

2.1.5 Outline of chapter

The remainder of this chapter is organized as follows: The experimental apparatus and samples are discussed in Sec. 2.2. Next, the results of the experiments and analysis of the data are presented in Sec. 2.3. Finally, a summary of the results is presented in Sec. 2.4.

2.2 EXPERIMENTAL

2.2.1 Luminescence experiment

Above band-gap excitation of the samples was provided by a mechanically chopped, continuous Spectra-Physics model 166 Ar ion laser. The laser beam was focused onto the sample, with a spot diameter of about 1 mm. The average power densities for the data presented here varied between 0.3 and 14.0 W cm^{-2}, although power densities of up to 2 kW cm^{-2} were obtained by increasing the laser power and focusing the laser spot down to a few tenths of a millimeter. Samples were immersed in liquid helium or cold helium gas in a Janis research dewar. A temperature sensor and heater mounted near the sample on the sam-

ple arm allowed temperature control.

The usual window material for luminescence experiments is quartz, but the transmission of quartz is very low for wavelengths longer than 3.0 to 3.5 μm,[15] making it unsuitable for work with HgCdTe. Sapphire, however, transmits well out to about 5.5 μm[15] so this was used for the inner windows. For work even farther out in the infrared, Irtran 2 (ZnS) could be used for the inner windows, which has a 70% transmission out to approximately 12 μm[15,16] All three of these materials were successfully epoxied to the Janis dewars to produce a seal that was vacuum tight at liquid helium temperatures. For the outer window, BaF_2 windows were used, which have 85% transmission over most of their range, and are useful out to ~ 13 μm.[15]

The light leaving the sample was then focused with BaF_2 lenses onto the aperture of a Spex 1269 or 1400 grating spectrometer. The slit width of the spectrometer was chosen to give energy resolution of about 1 meV in the photoluminescence spectra. The signal was detected with a SBRC solid state detector, InAs for the x = 0.48 material, and InSb for the x = 0.32 material. The signal was processed with a PAR 124A lock-in amplifier, using a signal from the mechanical chopper as the reference signal.

2.2.2 Sample description

Characterizing the sample impurity concentrations is important because some of the observed luminescence is impurity related. The samples were obtained from Santa Barbara Research Center, and we report the sample descriptions they furnished us.[17] Both x = 0.32 samples were grown by float zone refining of polycrystalline HgCdTe. After the crystals were sliced, they were gold plated and annealed in Hg vapor. This process doped the crystals with Au and reduced the number of Hg vacancies. The acceptor concentration in both of the processed

crystals is about 10^{15} cm^{-3}. The x = 0.48 crystals were grown by the solid state recrystallization method. Two of the samples were treated as described above, and have an acceptor concentration of 10^{15} and 10^{16} Au cm^{-3}, respectively. The third was not gold plated before it was annealed in Hg vapor, and the result is an n-type sample with 10^{15} cm^{-3} residual donors. For the p-type samples, the acceptors are either Au substitutional atoms or Hg vacancies.

2.3 RESULTS AND DISCUSSION

Figure 2.1 is an example of a luminescence spectrum from HgCdTe. It is included because it shows all of the lines that are observed in the samples. The figure shows luminescence intensity as a function of emitted photon energy, with excitation provided by an above band gap laser. The peak at highest energy is band-to-band luminescence, which is produced when free electrons and holes recombine to emit light. The peak at lowest energy is produced by a combination of two luminescence processes, donor-acceptor luminescence, and band-to-acceptor luminescence. Both are produced when an electron recombines with a bound hole, but the first involves a bound electron, and the second a free electron. As the temperature is increased, the free electron process is favored, because the donors can become thermally ionized at fairly low temperatures. The intermediate energy peak is produced by bound exciton recombination luminescence. While the other lines mentioned are found in all the samples studied, the bound exciton luminescence is observed in only two of the three x = 0.48 samples. All of these lines will be discussed in more detail below, and evidence for the line assignments will be presented.

2.3.1 Band-to-band line

The highest energy line in both the x = 0.48 and x = 0.32 material is attributed to a band-to-band transition. The peak at the highest energy in Fig. 2.2 shows

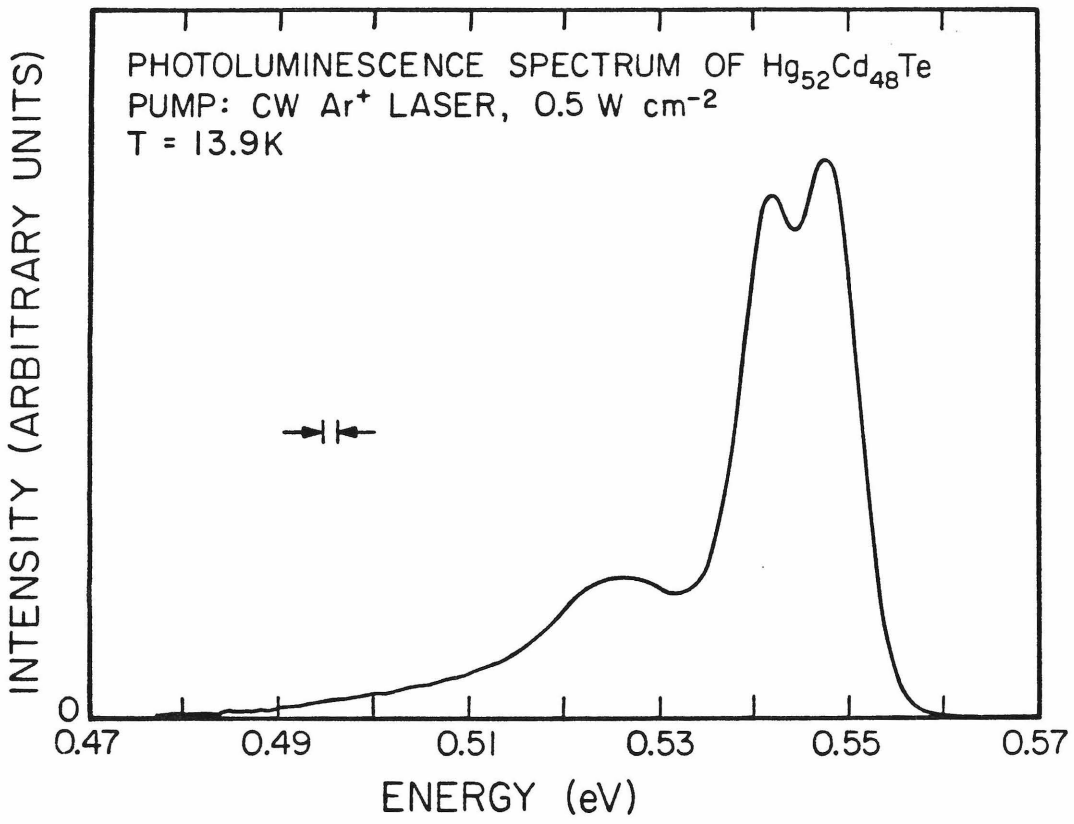

Figure 2.1: Spectrum of $Hg_{0.52}Cd_{0.48}Te$ showing photoluminescence intensity vs photon energy with the sample at 13.9 K. The high energy peak is due to band-to-band recombination. The low energy peak is due to a combination of donor-acceptor and band-to-acceptor luminescence. The intermediate energy line is due to bound exciton luminescence. The sample was n-type, with $N_D - N_A \sim 10^{15}$ cm^{-3}.

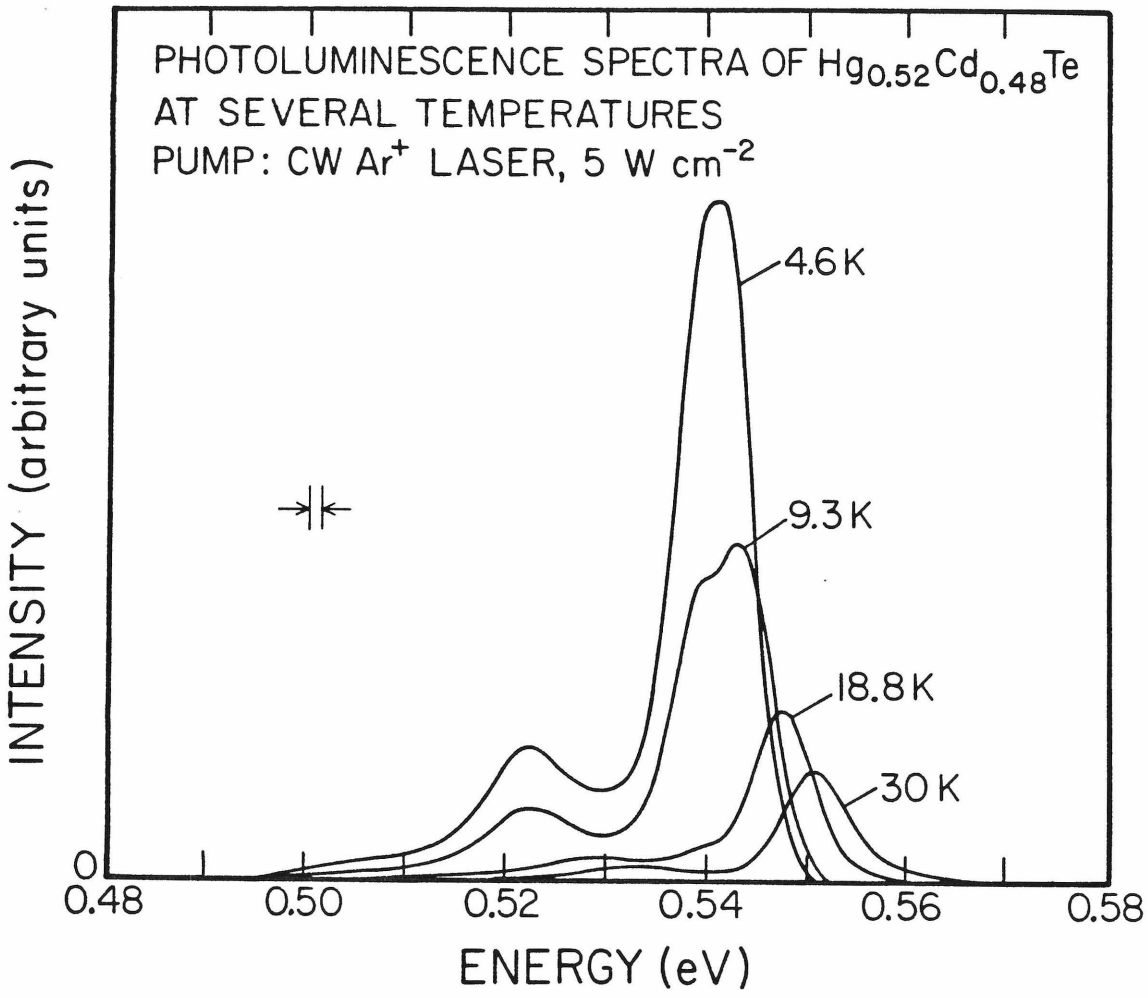

Figure 2.2: Spectra of $Hg_{0.52}Cd_{0.48}Te$ showing photoluminescence intensity vs photon energy with the sample at 4.6 K, 9.3 K, 18.8 K and 30 K, respectively. The high energy peak is due to band-to-band recombination, the low energy peak is due to donor-acceptor recombination at low temperature, and to band-to-acceptor luminescence above ~ 10 K. The intermediate energy line (shown most clearly in the 9.3 K spectrum) is due to bound exciton recombination. The sample was n-type, with $N_D - N_A \sim 10^{15}$ cm^{-3}.

this line in the 0.48 material, for several temperatures, and the peak at the highest energy in Fig. 2.3 presents similar data for x = 0.32 material. The qualitative features that characterize the line are the shift of the line to higher energy as temperature is increased, and the superlinear increase in intensity of the line as pump power is increased. The shift as temperature is increased implies that free carriers are involved in the transition. The superlinear increase in line intensity with pump power comes about because the band-to-band transition probability depends on the product of hole and electron concentrations, both of which increase as pump power is increased. Another factor suggesting that this transition is band-to-band is that no luminescence is observed with higher photon energy. In the remainder of this section, we will first describe these observations in detail, then we will discuss a model for the transition that explains most of the data.

Both Fig. 2.2 and Fig. 2.3 clearly show the high-energy luminescence band shifts toward higher energy as temperature is increased. This information is summarized for several pump powers in Figs. 2.4 and 2.5. In both figures, energy of the line peak is plotted against temperature, with the points for a given luminescence band at one pump power connected as an aid to the eye. Figure 2.4 shows these data for the x = 0.48 material. The top three curves, labeled band-to-band, show the behavior of this line for three different pump powers. The slope of each of these curves is approximately 3 k_B, where k_B is Boltzmann's constant, 0.0862 mev K^{-1}. The top three lines in Fig. 2.5 also yield a slope of approximately 3 k_B, for the shift of the band-to-band line in x = 0.32 materials.

The band-to-band intensity increases rapidly as pump power increases. In material of both compositions, the rate of increase is faster than linear at most temperatures and pump powers for which measurements were made. In

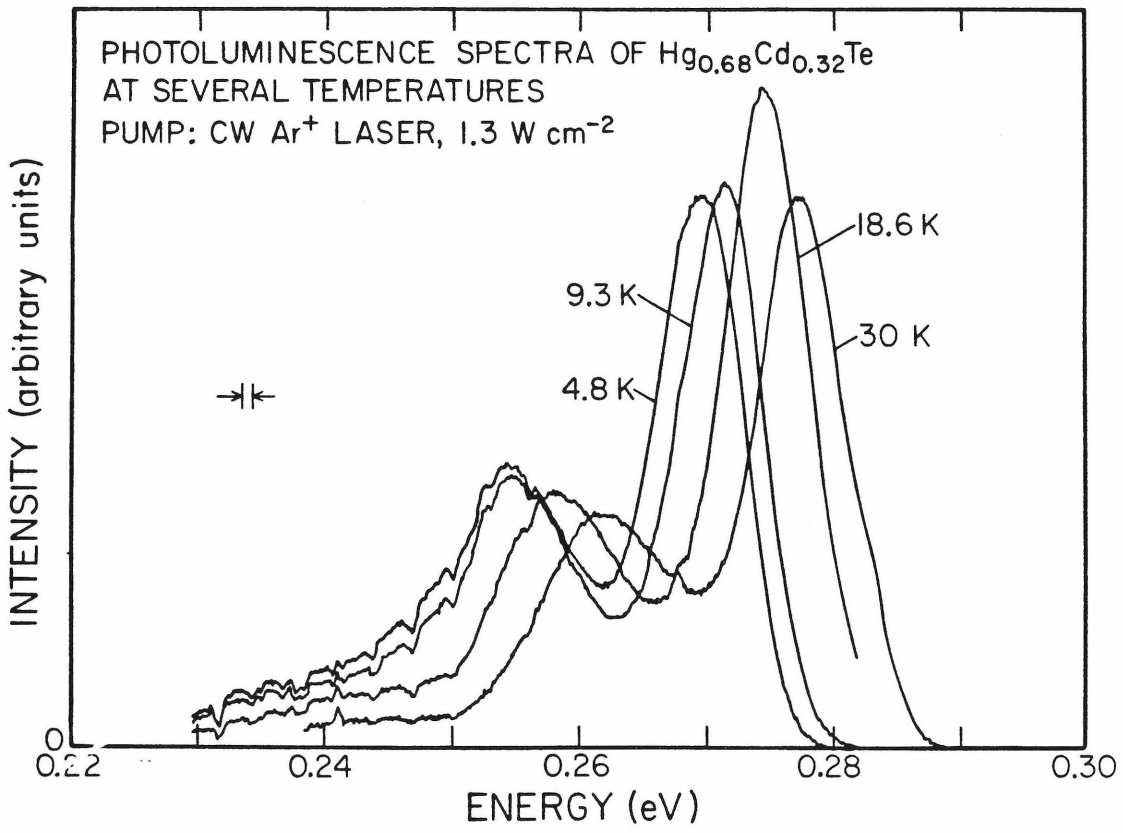

Figure 2.3: Spectra of $Hg_{0.68}Cd_{0.32}Te$ showing photoluminescence intensity vs photon energy with the sample at 4.8 K, 9.3 K, 18.6 K, and 30 K, respectively. The high energy peak is due to band-to-band recombination, and the low energy peak is due to donor-acceptor recombination at low temperatures, and to band-to-acceptor recombination above ~ 10 K. The structure seen mostly on the lower energy peak, is due to atmospheric water vapor absorption. The sample was p-type, with $N_A - N_D \sim 10^{15}$ cm^{-3}.

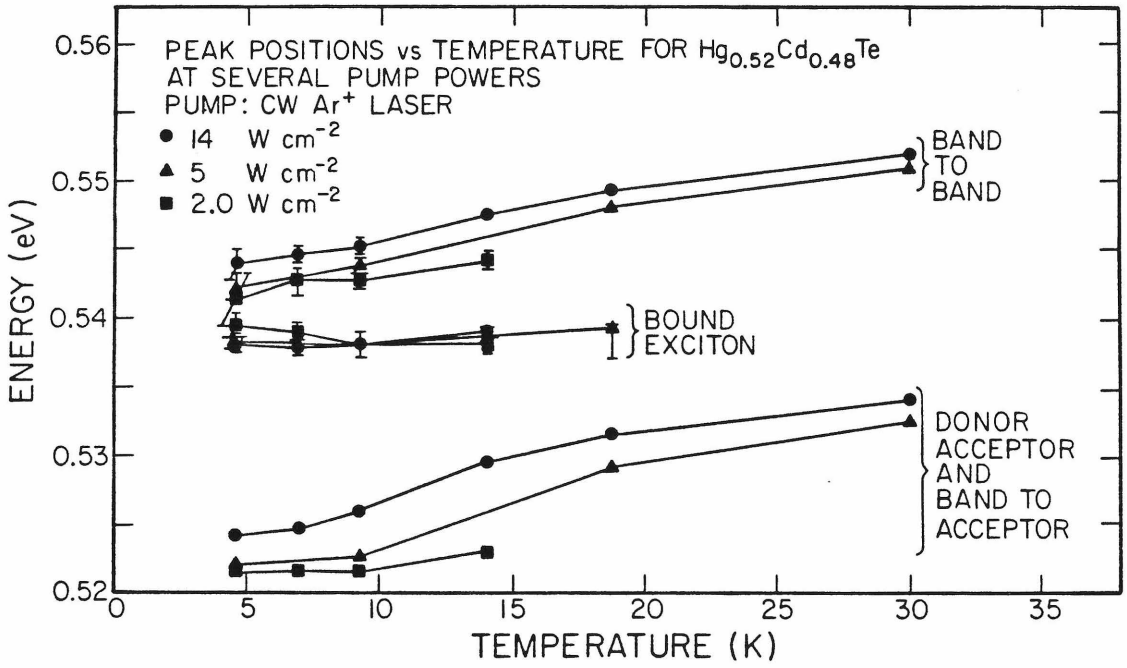

Figure 2.4: Summary of luminescence-band peak energies vs temperature of $Hg_{0.52}Cd_{0.48}Te$ at three different pump powers for the sample of Fig. 2.2. The lines between data points are drawn as a visual aid, and connect points measured at different temperatures for one type of luminescence band at one pump power. Error bars are given where significant; the uncertainty is due to overlap between bands.

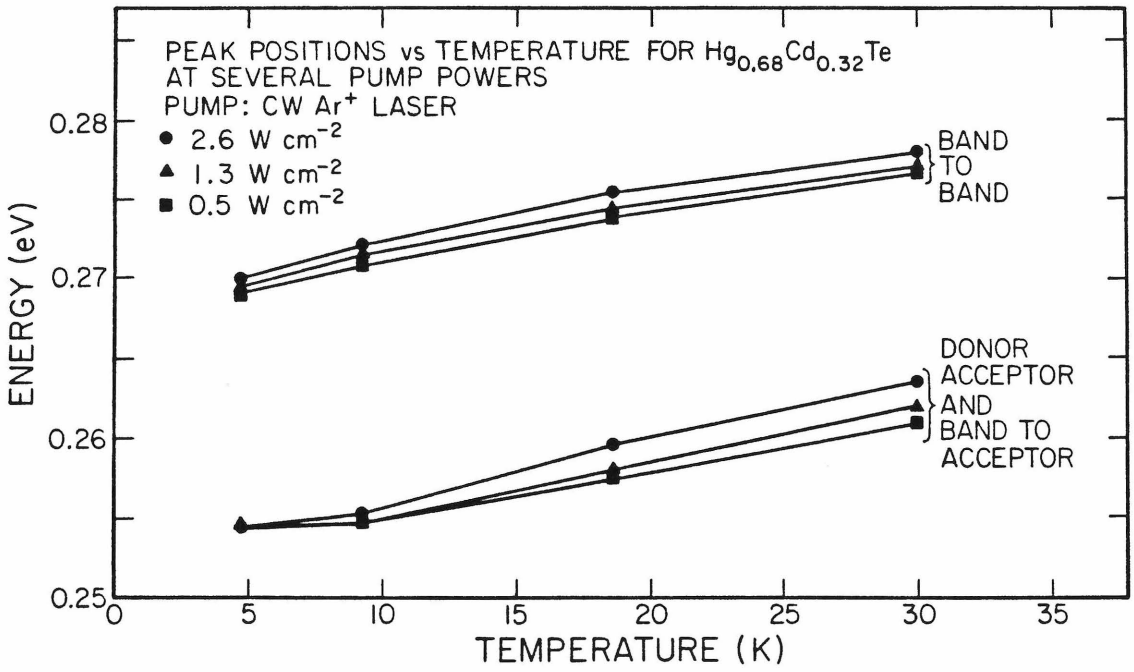

Figure 2.5: Summary of luminescence-band peak energies vs temperature of $Hg_{0.68}Cd_{0.32}Te$ at three different pump powers for the sample of Fig. 2.3. The lines between data points are drawn as a visual aid, and connect points measured at different temperatures for one type of luminescence band at one pump power.

the x = 0.48 material at 30 K (where the results are not complicated by overlap with the bound exciton line) the band-to-band intensity increases by a factor of 4 when pump power is increased by ~ 2.5. In the x = 0.32 material, the intensity at 5 K increases by a factor of 9 when pump power is increased by a factor of 5. (Although at 30 K in this sample, the increase is down to slightly sublinear with pump power). Therefore over the range of temperatures and pump powers for which we took data, the rate of increase of the band-to-band line intensity ranged from slightly sublinear to super linear, but always less rapidly than the square of the pump power.

The model for the transition that best accounts for the shape, peak shift, and intensity variation of the line, is that the free carriers act as an electron-hole plasma, with recombination proceeding without wave-vector conservation. Under the assumptions of our model, an electron-hole droplet-like lineshape[18] results:

$$I(\hbar\omega) = \int_0^{\hbar\omega - E_g} d\varepsilon \frac{\varepsilon^{\frac{1}{2}} (\hbar\omega - \varepsilon - E_g)^{\frac{1}{2}}}{[1+\exp((\hbar\omega - \varepsilon - E_g - \mu_h)/k_B T)][1+\exp((\varepsilon - \mu_e)/k_B T)]}, \quad (2.1)$$

where $I(\hbar\omega)$ is luminescence intensity at photon energy $\hbar\omega$, E_g is band gap energy, μ_e and μ_h are electron and hole chemical potentials, respectively, and $k_B T$ is Boltzmann's constant times the sample temperature. This equation fits the high energy line fairly well at 20 and 30 K, although it is somewhat too narrow for the data at lower temperatures. However, the width of the lines observed at lower temperatures is approximately that which would be produced by compositional variation across the width of the pump beam. This compositional broadening was not included in the theoretical lineshapes; however, if it were included, the lineshape predicted by the model would probably agree with the data over the entire temperature range.

Figure 2.6 shows the result of a fit at 30 K for one spectrum of the x = 0.48 material. Band gap energy and carrier density were varied to obtain the fit, with inputs being temperature (T = 30 K, the bath temperature in the experiment), and electron and hole effective masses (m_e^* = 0.04, m_h^* = 0.5, from Ref. 1). The agreement between theory and data, while not exact, is much better than could be obtained for different models, such as for an exciton gas, or an electron-hole plasma in which recombination proceeds with wavevector conservation. Furthermore, the carrier density, which is the only variable that affects the shape of the predicted line, is not an entirely free parameter, since it can be estimated from the pump-laser power density. The value of the carrier density used to generate the fit is consistent with that estimated from the power density used in the experiment.

The model can account for most of the large peak shift that is observed in the data as temperature is changed. In the nondegenerate limit (high temperature and low density, which is approximately valid for this experiment), Eq. 2.1 can be integrated analytically to give:

$$I(\hbar\omega) = \frac{\pi}{8}(\hbar\omega - E_g)^2 \exp(-(\hbar\omega - E_g)/k_B T)\, \exp((\mu_e + \mu_h)/k_B T). \qquad (2.2)$$

The maximum of this lineshape occurs at $\hbar\omega = E_g + 2k_B T$, so as temperature is increased, the maximum shifts to higher energies at a rate equal to 2 k_B. This shift is smaller than the 3 k_B observed experimentally, but there are several mechanisms which can provide additional peak shift.

One such source of additional shift is that the band gap may shift slightly in the temperature range covered. Above 20 K, the shift has been measured by other groups to be linear with temperature, and is ~ 0.2 meV K^{-1} for the x = 0.32 material, and less than 0.05 meV K^{-1} for the x = 0.48 material.[1,19,20]

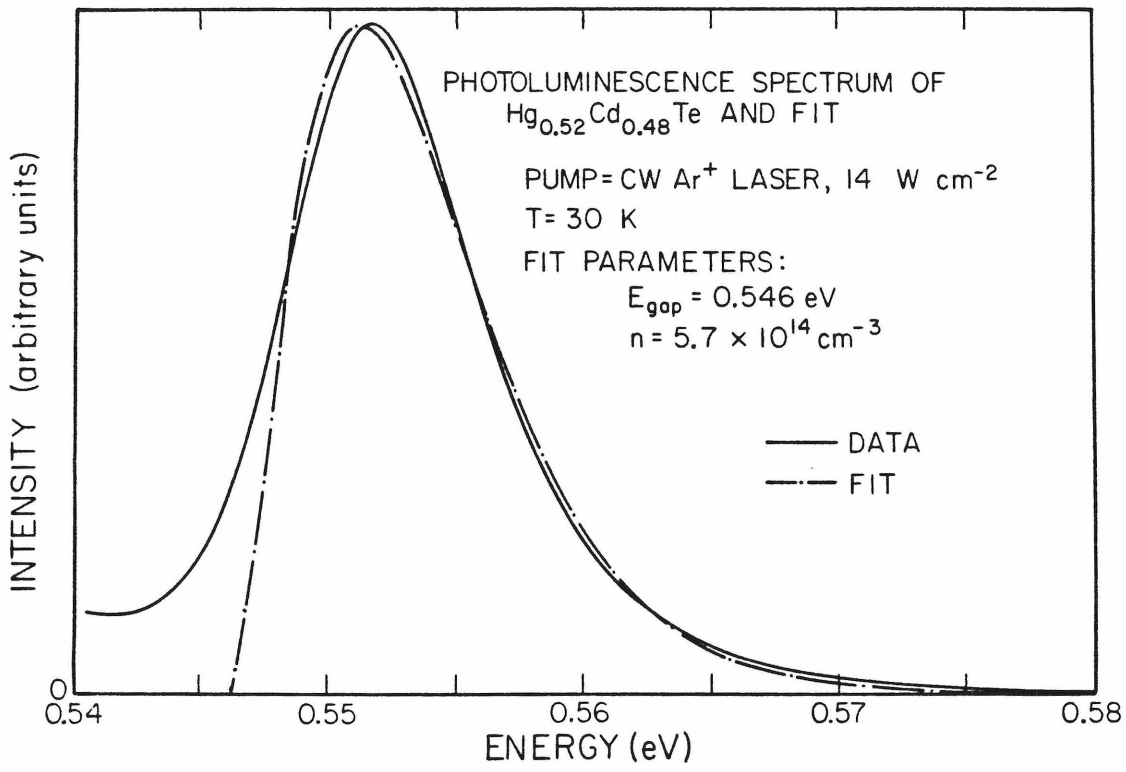

Figure 2.6: Photoluminescence spectrum of the high energy peak of $Hg_{0.52}Cd_{0.48}Te$ for the sample of Fig. 2.1 and 2.2, and a fit to the data. The fit is appropriate to an electron-hole plasma recombining without wavevector conservation. Three parameters, the carrier density, band-gap energy, and peak intensity, were varied to obtain the fit. The temperature used in the expression for the lineshape was 30 K, and electron and hole masses used were 0.04 m_e and 0.5 m_e, respectively.

Data are not available for lower temperatures; hence, we have had to estimate the shift at temperaturs below 20 K. For many semiconductors, the rate of band gap shift with temperature decreases below 20 K.[21] Therefore, the high temperature values for the rate of shift are likely to be either reasonable approximations to the band gap shift, or upper limits to it. Using the values at 20 K we estimate a band gap shift between 5 and 30 K (the range over which we took data) of less than 4.5 meV for the x = 0.32 material, and less than 1 meV for the x = 0.48 material. While band gap shift and line shift as predicted by Eq. 2.2 could account for all the observed shift of the line-peak energy with temperature in x = 0.32 material, we need to account for an additional 2 meV of shift in the 0.48 material. Since this remaining discrepancy is probably larger than the error bars on the measurement, we suggest one final source of additional shift. The peak shift of $2k_B$ assumes a constant carrier density as temperature is changed. This, however, is not entirely accurate since the hole density increases as acceptors become thermally ionized. This increase in free carrier density can contribute a small shift of the band-to-band line to higher energy. In conclusion, these two mechanisms, together with the peak shift predicted by our model, can adequately account for all the peak shift observed in x = 0.32 material. They may predict a shift slightly smaller than that observed in the x = 0.48 material, but they do account for most of the shift that is observed.

The super-linear increase of line intensity with pump power provides additional evidence for a band-to-band transition of the type discussed earlier. This can be seen by some simple rate equation arguments. The band-to-band transition probability can be written as $An_e n_h$, where n_e and n_h are the free electron and hole concentrations, respectively, and A is a constant independent of temperature and pump power. Since both n_e and n_h increase with pump

power, a super-linear increase of the product is expected.

This section will be closed with a discussion of the assumptions involved in the proposed model. The lack of wavevector conservation in the band-to-band transition has been used successfully to explain the gain spectrum of GaAs,[22,23] where free carrier and impurity scattering are large enough to relax the wavevector selection rules. The model should apply to HgCdTe, but perhaps for slightly different reasons. The impurity and carrier concentrations are somewhat lower in the HgCdTe samples than in the GaAs lasers considered in Refs. 22 and 23. In the alloy the random fluctuations in concentration can also act as scattering centers for electrons,[10] and so lead to relaxation of the wavevector selection rules. However, the major justification for invoking recombination without wavevector conservation is that it helps to explain the large shift of this line with temperature, and can fit the shape of the line for the higher temperature spectra.

Another assumption in all the models considered above for the band-to-band line shape is that the band edges were parabolic. This, in turn, predicts a sharply defined absorption edge. It is very likely that the band edge electronic states are not well defined by this simple model, however, because the absorption edge for HgCdTe is fit by a modified Urbach tail in HgCdTe with a composition of $x \sim 0.2$.[24] This exponential behavior of the absorbion edge may be a reflection of compositional inhomogeneities on a macroscopic scale. However, it could also be a sign of disorder on a microscopic scale as discussed in the introduction. The states formed by compositional fluctuations can lead to states in the gap.[6,8,9]. However, this tailing of states into the gap was not included in the attempted fits of the band-to-band lineshape. Since the model is able to fit the data, it implies that for the carrier density in these experiments, the majority of

electronic states do not come from the tail in the density of states distribution. Instead, they come from a part of the bands which is described by the zero order virtual crystal approximation.[6] Therefore, the disorder does not affect the band-to-band line shape through the density of states, but by changing the transition matrix element. The compositional fluctuations serve as scattering centers to allow non-momentum conserving transitions.

2.3.2 Electron-to-bound hole band

The low energy peak, observed in all the spectra at all temperatures, is produced by electrons recombining with holes bound to acceptors, processes which have been extensively investigated in other materials.[25,26] The leftmost band in Fig. 2.2 shows this luminescence in x = 0.48 material, at several temperatures, and Fig. 2.3 shows similar data for x = 0.32 material. The same qualitative behavior is demonstrated in material of each composition. The peak position does not change in going from ~ 5 to ~ 10 K, then shifts substantially from 10 to 30 K. At the lowest temperatures studied, the electrons are bound to donor atoms, but at higher temperatures (above about 10 K), most of the donors are thermally ionized (donor binding energies are estimated to be approximately 2 and 3.5 meV for x = 0.32 and 0.48 material, respectively, from the hydrogenic model[1]) and the luminescence is caused by conduction band electrons recombining with bound holes. The presence of a significant donor-acceptor luminescence line indicates the material is compensated, although the degree of compensation is difficult to estimate.

The shape of the line is similar in both materials, with a long tail on the low energy side. On spectra taken at lower pump power, in which the band-to-band line is not as prominent, the low energy line clearly appears asymmetric, with the high energy edge falling off much more sharply than the low

energy side. This impurity related line is somewhat broader than the higher energy band-to-band line. There are several reasons for the breadth. The first is that the energy of luminescence depends on the distance between the impurities, since part of the line is due to donor-acceptor recombination. The second is the Urbach tail behavior mentioned earlier for the absorption edge in HgCdTe, which can produce tails on band related luminescence lines. This is probably the origin of the long low energy tail seen in all the spectra. Finally, the impurities see a distribution of environments since, instead of being in a perfect lattice, they are in an alloy. Smith[11] has calculated that this would give a width of about 10 meV to an acceptor level. (The corresponding broadening for a donor level world be much smaller, simply because the donor binding energy itself is so small.) These broadening mechanisms are responsible for the fact that the low energy threshold of the bands is not $E_g - E_A - E_D$ (E_A and E_D are the acceptor and donor binding energies, respectively), corresponding to luminescence produced by donor-acceptor pairs at infinite separation. The luminescence tail extends much farther to low energy than could be accounted for by reasonable estimates of the impurity ionization energies. Because of this long low energy tail, and the overlap with the band-to-band line on the high energy edge, we did not attempt a fit of this line.

The shift of the peak with temperature provides most of the information needed to understand the origin of the luminescence, however. The shift in the peak position of this line is caused by somewhat different mechanisms than for the band-to-band line. Figures 2.4 and 2.5 show the shift in the peak position of this line as a function of temperature for several pump powers. The most important feature of this shift is that it is not uniform with temperature, and does not shift significantly below 10 K, for any pump power. The peak position then shifts rapidly above 10 K. This sudden shift is consistent with a

change from a transition involving mostly bound electrons recombining with the bound hole to a transition involving free electrons. The band-to-acceptor line by itself should shift with $\sim 1/2\ k_B T$ in addition to band gap shift,[26] since in this case the shift is caused by the thermal excitation of only one of the particles, the electron. The lower curves on Figs. 2.4 and 2.5 indicate it may shift somewhat more than this, but much of the excess shift is probably expained by the ionization of the electron.

Since this low energy line is impurity related, it should decrease in intensity relative to the higher energy band-to-band line as pump power is increased. This can be seen by again referring to the simple rate equation model. As mentioned earlier, the band-to-band probability goes as $An_e n_h$. The band-to-acceptor probability goes as $Bn_e N_a$, where N_a is the number of neutral acceptors and B is another constant. At the low temperatures of the experiment, with the $\sim$ 15 meV acceptor ionization energy, almost all of the acceptors are neutral: from model rate equaton calculations we estimate N_a does not change by more than 10% in the temperature range studied. Therefore, the ratio of band-to-band to band-to-acceptor intensity should go as $\sim constant\ n_h$, which increases with pump power. This is the behavior observed in the experiment. For x = 0.32, the ratio increases by 25 to 100% (depending on temperature) as pump power is increased by a factor of 5. For x = 0.48, the situation is complicated by overlap with the bound exciton line, but the results are qualitatively similar.

Donor and acceptor ionization energies can be estimated from the separation between the peaks of the luminescence lines. Overlap between lines and low energy tails make it impractical to use the low energy thresholds for determination of these energies. However, allowing for the estimated linewidths,

we can give limits for the donor and acceptor binding energies. We have estimated the donor binding energy to be 1.0 ± 1.0 meV in x = 0.32 material, and 4.5 ± 2.0 meV in x = 0.48 material. For acceptors, the corresponding energies are 14.0 ± 1.5 meV and 15.5 ± 2.0 meV. This agrees approximately with the values listed in Ref. 3: the authors estimate values of the acceptor ionization energy for x ~ 0.3 material of 13 meV from the luminescence data and 20 meV from the Hall data. For x = 0.5 material, they estimate 25 meV from luminescence measurements. Our values agree very closely with a more recent estimate of E_A from temperature dependence of Hall data which included the effect of compensation.[14] They checked their estimates of E_A by doing far infrared photoconductivity measurements, and deduced 14.0 ± 1.0 meV for x = 0.4 material.[14]

2.3.3 Bound exciton

The last luminescence line we observe has the characteristics of bound exciton luminescence. This line is clearly resolved in the luminescence spectrum shown in Fig. 2.1. The 9.25 K spectrum on Fig. 2.2 also shows this third line reasonably clearly. On the 4.6 K spectrum, it overlaps the band-to-band line and is difficult to identify. Also, the intensity has dropped sufficiently to make it difficult to resolve on the 18.8 K sample. This intermediate energy line was seen only in two out of three x = 0.48 samples, the p-type 10^{16} cm^{-3} sample, and the n-type 10^{15} cm^{-3} sample. It was not seen in the other x = 0.48 sample (p-type, 10^{15} cm^{-3}), nor in either of the x = 0.32 samples.

Since the line was not seen in all of the x = 0.48 samples studied, composition was not the only factor that determined whether or not the line was observed in the luminescence spectrum. However, there are two reasons to expect a bound exciton line should be easier to observe in material of higher composition. The first involves the lifetime expected for bound excitons in this

material. Osbourn and Smith[7] have performed a calculation of the radiative and Auger lifetime of bound excitons in HgCdTe as a function of compositon. They find that the probability of a radiative transition increases with increasing Cd concentration. On the other hand, the Auger probability (over the range of interest in the experiments described here) decreases with increasing Cd concentration. The crossover point occurs at x = 0.4. According to their calculation, the radiative efficiency for a bound exciton in x = 0.48 material is 90%, compared to an efficiency of 20% in x = 0.32 material, for which we observe no bound exciton luminescence. A second factor which would make it less likely to observe a bound exciton in x = 0.32 material is that the exciton Bohr radius is somewhat larger in x = 0.32 material that in the x = 0.48 material. This means that, for a fixed impurity concentration, the exciton would overlap more impurities in the x = 0.32 material than in the x = 0.48 material.

Figure 2.4 shows the shift in the peak position of the bound exciton as a function of temperature for several different pump powers. As can be seen from the spectra shown in Fig. 2.2, the bound exciton line is difficult to resolve from the band-to-band line. Although it is more clearly resolved at other pump powers and temperatures, it was necessary to use a fitting routine to determine the position of the lines when they overlapped substantially. For this purpose, we used a two Gaussian fitting routine, and did not attempt to fit the tails of the lines. Although this procedure did not reproduce the exact shape of the lines, it did allow a reasonable estimate of the position of the lines. The error bars reflect a range of positions for the peaks that gave reasonable fits. To within the accuracy of the measurements, the line does not shift as either pump power or temperature is changed. This is an important piece of evidence indicating that the line is a bound exciton line, since both carriers must be bound if the energy of the luminescence does not shift as temperature is raised.

The width of the line also supports the bound exciton interpretation of the luminescence. Figure 2.7 shows spectra taken on a different x = 0.48 sample in which the bound-exciton line was much more intense than the band-to-band line at the lowest temperatures studied. In this case, the impurity concentration was high enough, and pump power low enough, that most available electrons and holes could become bound to impurity centers before recombination, rather than recombine as free carriers. These data, therefore, allow an unambiguous determination of the line width. We determined the width to be 6 meV from the 4.8 K spectrum shown in Fig. 2.7. This agrees with the width of ~ 5 meV for bound-exciton recombination luminescence calculated by Smith[11] taking into account the broadening induced by the distribution of environments around the acceptors.

Finally, the drop in intensity and position of this intermediate energy line are characteristic of a weakly bound state. At low temperatures, the line is only 2 or 3 meV below the band-to-band line, indicating an ionization energy of this magnitude. The rapid decrease in intensity of the line with respect to both of the other lines also indicate that the ionization energy is small. The only other alternative to the bound exciton is a free hole recombining with a weakly bound electron. This possibility is eliminated by the lack of shift of the line with temperature mentioned above.

2.3.4 Spatial variations in band gap

The samples studied showed a lateral concentration gradient from one side of the wafer to the other. Since the concentration determines the band gap, the change in concentration was reflected in a shift of the luminescence lines in energy. Figure 2.8 shows typical luminescence data for a sample of x = 0.32 material. The three different spectra were collected under identical conditions,

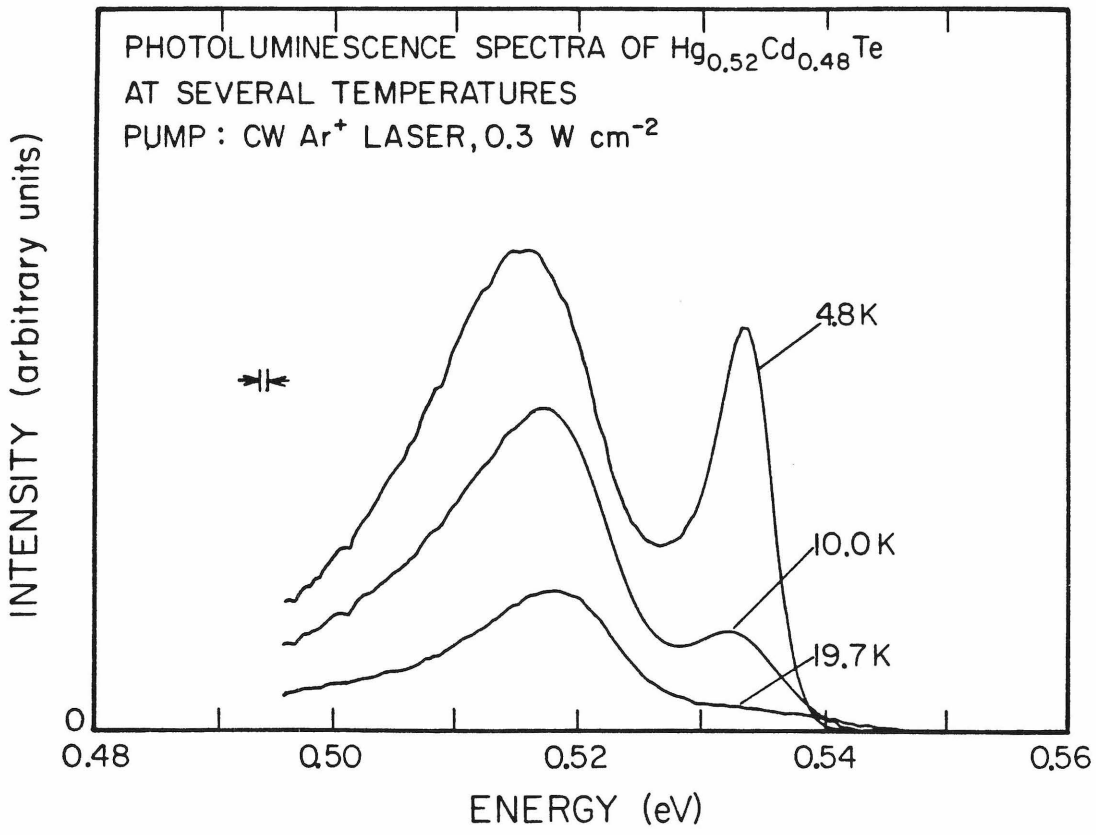

Figure 2.7: Spectra of $Hg_{0.52}Cd_{0.48}Te$ showing photoluminescence intensity vs photon energy with the sample at 4.8 K, 10.0 K, and 19.7 K, respectively. These spectra are for a different sample (p-type, $N_A - N_D \sim 10^{16}$ cm^{-3}), and were taken at lower pump power than the spectra in Fig. 2.2. The band-to-band line is not visible at these temperatures, and the high energy line is due entirely to bound exciton recombination luminescence.

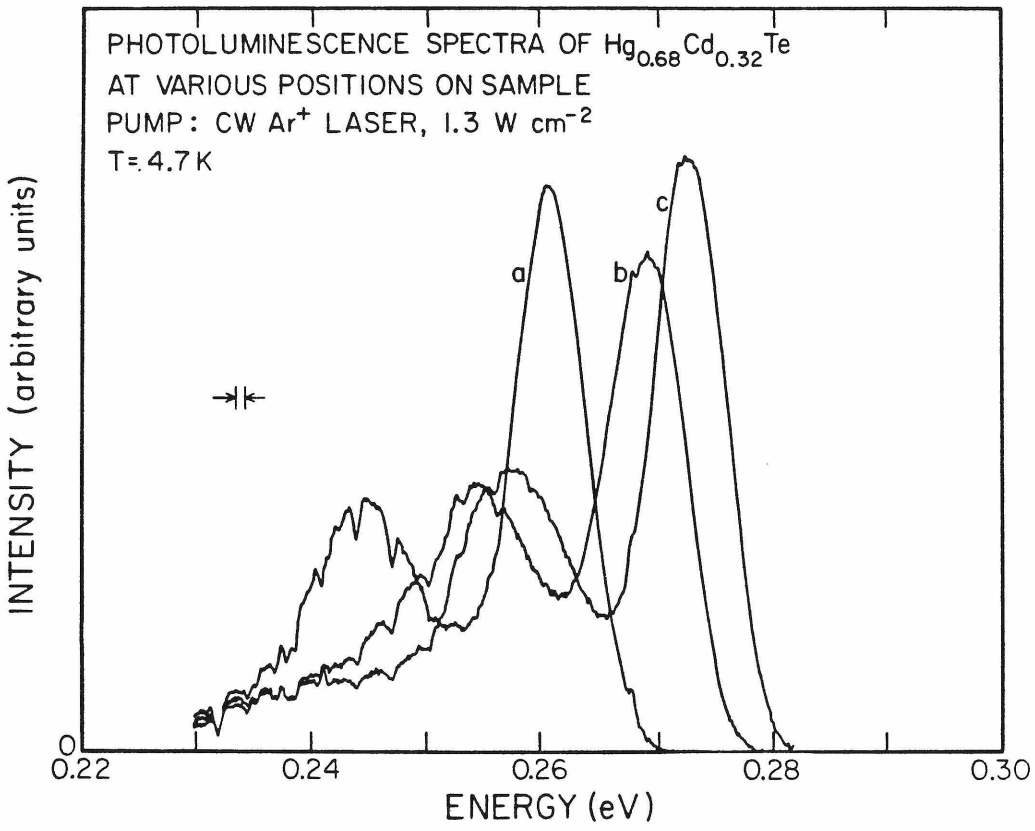

Figure 2.8: Spectra of $Hg_{0.68}Cd_{0.32}Te$ showing photoluminescence intensity vs photon energy for the sample of Fig. 2.3. For spectrum b, the pump laser was 1.0 mm above its position for spectrum a, and for c, 2.5 mm above its position for spectrum a. The shift in energy between a and c implies a shift in composition of 0.03 cm^{-1}.

except that the sample was moved with respect to the pump laser and spectrometer, so that the luminescence came from a different part of the sample in each case. Assuming that all of the shift in luminescence energy was caused by band gap shift, and using published fits relating band gap energy to composition,[1] a change in composition of 0.03 cm^{-1} is implied. This means that luminescence experiments can provide a fairly sensitive means of monitoring compositional changes across the surface of HgCdTe wafers. The position of the luminescence lines in our spectra can be determined to within about 1.0 meV, which would allow a resolution of 0.0006 for measurement in a composition change from one point to another. Some additional uncertainty would be added to the measurement because of uncertainty in the relationship between composition and band gap. The formulas compiled in Ref. 1 give a spread of 15% in the compositional changes implied by a given band gap shift.

The compositional gradient may have contributed to the width of the luminescence lines, since the spot size of the pump laser was several millimeters in diameter. A 2 mm spot causes a 4 meV line width because of the gradient alone. This should be regarded as a lower limit on the width, however, since the gradient was measured over a distance of many millimeters and implies nothing about local, but still macroscopic, fluctuations in composition, which could contribute even more to the line width.

2.3.5 Laser induced damage

High intensity laser irradiation was found to damage one of the samples. Surface damage occurred while irradiating a p-type $x = 0.48$ sample with an estimated 2 kW cm^{-2} continuous laser beam, while the sample was in contact with a sample block at 5 K. The damage occurred suddenly, as indicated by a sudden loss of luminescence signal. The sample so damaged had a small pit of

approximately the same size as the laser beam (about 0.1 mm in radius) with a depth of about 0.1 mm.

2.4 SUMMARY OF RESULTS

In this paper we have described our observations of luminescence spectra of $Hg_{1-x}Cd_xTe$, for x = 0.32 and x = 0.48. We observed band-to-band, band-to-acceptor, donor-acceptor, and bound exciton recombination luminescence.

The band-to-band line shape, and variation of intensity with pump power, implies an electron-hole plasma in which recombination proceeds without wavevector conservation. This model indicates that a perfect crystal density of states may be used for the electrons and holes involved in the transition. The effect of disorder is to allow non-wavevector conserving recombination of the electron and hole.

Donor and acceptor ionization energies have been estimated from the luminescence data. For E_A, we estimate 14.0 ± 1.5 meV for x = 0.32 material and 15.5 ± 2.0 for x = 0.48 material. The acceptor is probably either a Au substitutional atom or alloy vacancy. This agrees well with values obtained from infrared photoconductivity data and temperature dependence of Hall measurements in which compensation was taken into account.[14] We estimate E_D = 1.0 ± 1.0 and 4.5 ± 2.0 meV in x = 0.32 and x = 0.48 material, respectively, which is consistent with values calculated in the hydrogenic model.[1] The identity of the donor is unknown. The presence of the donor-acceptor luminescence band indicates our samples are compensated.

The observation of the bound exciton luminescence in the x = 0.48 material is consistent with the calculation by Osbourn and Smith[7] showing a radiative efficiency of 90% for the bound exciton in HgCdTe of this composition.

We did not observe the line in x = 0.32 material, although this does not mean bound excitons do not occur in this material, since we did not see the bound exciton line in one of the x = 0.48 samples. However, the absence of the line in x = 0.32 material is consistent with the Osbourn-Smith estimate of a much lower radiative efficiency of 20% for bound exciton recombination in that material.

Finally, luminescence could be utilized as an easy, non-damaging means of monitoring compositional changes across the surface of a HgCdTe wafer. The area sampled can be made essentially as small as the spot size of the laser. Unlike an absorption measurement, it can be made on a sample of any thickness. Finally, the technique yields very reasonable signals at laser pump power densities two or three orders of magnitude below a power density that would damage the material. This is not necessarily true for techniques that use electron-beams as a probe of Hg and Cd concentrations.

REFERENCES

1. See, for example, R. Dornhaus and G. Nimtz, in *Springer Tracts in Modern Physics*, Vol. 78, edited by G. Hohler (Springer-Verlag, Berlin, 1976), pp. 1-112.

2. J. I. Pankove, *Optical Processes in Semiconductors* (Dover, New York, 1971), p. 413.

3. C. T. Elliot, I. Melngailis, T. C. Harman, and A. G. Foyt, J. Phys. Chem. Solids **33**, 1527 (1972).

4. V. I. Ivanov-Omskii, V. A. Mattseva, A. D. Britov, and S. D. Sivachenko, Phys. Status Solidi(a) **46**, 77 (1978).

5. L. Nordheim, Ann. Physic **9**, 607 and 641 (1931).

6. R. H. Parmenter, Phys. Rev. **97**, 587 (1955).

7. G. C. Osbourn and D. L. Smith, Phys. Rev. B **20**, 1556 (1979).

8. Zh. I. Alferov, E. L. Portnoi, and A. A. Rogachev, Sov. Phys. Semicond. **2**, 1001 (1969).

9. S. D. Baranovskii and A. L. Efros, Sov. Phys. Semicond. **12**, 1328 (1979).

10. L. Makowski and M. Glicksman, J. Phys. Chem. Solids **34**, 487 (1973).

11. D. L. Smith, unpublished.

12. R. J. Elliot, J. A. Krumhansl, P. L. Leath, Rev. Mod. Phys. **46**, 465 (1974).

13. D. Stroud, H. Ehrenreich, Phys. Rev. B **2**, 3197 (1970).

14. W. Scott, E. L. Stelzer, and R. J. Hager, J. Appl. Phys. **47**, 1408 (1976).

15. J. A. Jamieson, R. H. McFee, G. N. Plass, R. H. Grube, R. G. Richards, *Infrared Physics and Engineering* (McGraw-Hill, New York, 1963), Chapter 7.

16. Kodak Publication U-72, *Kodak Irtran Infrared Optical Materials*, pp. 1-52.

17. P. Bratt and R. Cole private communication.

18. Ya. E. Pokrovsky, Phys. Status Solidi(a) **11**, 385 (1972).

19. M. W. Scott, J. Appl. Phys. **40**, 4077 (1969).

20. J. L. Schmit and E. L. Stelzer, J. Appl. Phys. **40**, 4865 (1969).

21. Y. P. Varshni, Physica **34**, 149 (1967).

22. G. Lasher and F. Stern, Phys. Rev. **133**, A553 (1964).

23. E. Gobel, Appl. Phys. Lett. **24**, 492 (1974).

24. E. Finkman and Y. Nemirovsky, J. Appl. Phys. **50**, 4356 (1979).

25. See, for example, J. J. Hopfield, D. G. Thomas, and M. Gershenzon, Phys. Rev. Lett. **10**, 162 (1963); D. G. Thomas, J. J. Hopfield, and W. M. Augustyniak, Phys. Rev. **140**, A202 (1965); M. R. Lorentz, T. N. Morgan, and A. P. Pettet, in Proceedings on the Physics of Semiconductors, edited by S. M. Ryvkin (Nauka, Leningrad, 1968), p. 495.

26. See, for example, D. M. Eagles, J. Phys. Chem. Solids **16**, 76 (1960).

CHAPTER 3

TRANSIENT DECAY OF BOUND MULTI-EXCITON LINES IN Si:P

3.1 INTRODUCTION

3.1.1 Background

The luminescence spectrum of doped Si contains series of sharp lines that are very near the band gap in energy. These lines are associated with the bound exciton line, and are thought to be caused by electron-hole recombination within neutral, bound multi-exciton complexes. This general interpretation is fairly well established; however, to do so, and to attempt to formulate a more detailed theory of the states, required extensive experimental[1–13] and theoretical investigations.[4,14–16] A shell model[15,16] was proposed to describe the states, but this explanation was very controversial at the time our experiments were carried out. An accurate measurement of the decay behavior of the luminescence was regarded as a very decisive test of a shell model prediction. Our experiments provided the first measurements accurate enough to show the decays were consistent with the prediction of the model.

Several replicas of the luminescence lines are observed. The highest energy replica is produced when recombination occurs without the emission of a phonon. Phonon-assisted recombination can also occur, and these lines are shifted from their no-phonon counterparts by the energy of phonons with wavevector equal to that of the conduction band minimum. For donors,[7,8,13] one set of lines, labeled the α series,[7,8] is observed in both no-phonon and phonon-assisted transitions. An additional set of lines, labeled the β series,[7,8] is observed in the phonon assisted transition. These lines are shown in Fig. 3.1, for silicon doped with the donor phosphorous. The spectrum on the top shows the α series of the no-phonon transition. The α series appears again in the bottom spectrum, with each line spaced from its no-phonon replica by a transverse optical phonon energy. The additional lines seen in this lower spectrum are the β series of lines.

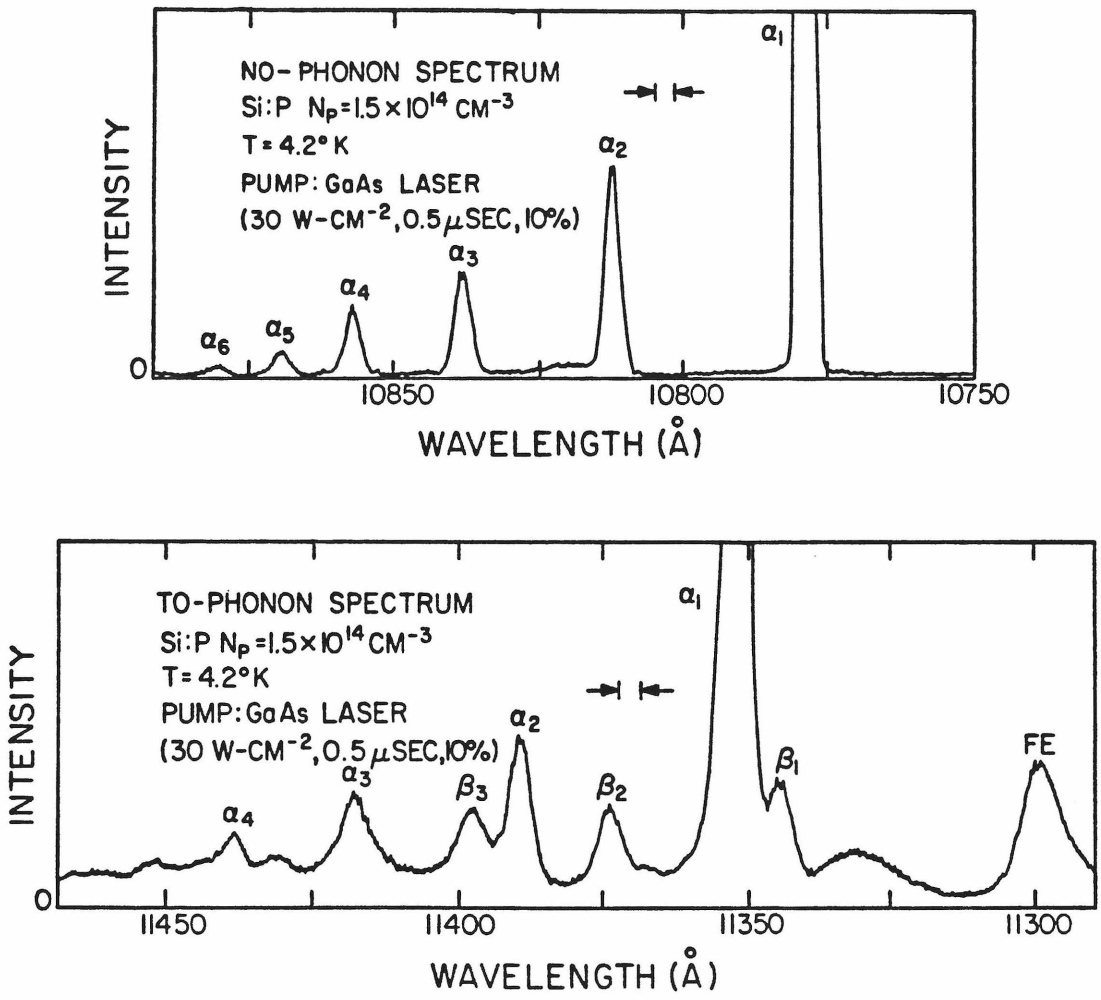

Figure 3.1: The photoluminescence spectrum of Si:P. The upper spectrum spans the energy range of the no-phonon replica. The lower spectrum spans the energy range of the transverse and longitudinal optical phonon replica.

Both the α and β series of lines have been interpreted in terms of the shell model[15,16] mentioned above. In this model, the electrons fill the single particle states of the donor and the holes fill the single particle states of the acceptor. The single particle states in Si, however, are slightly more complicated than for a semiconductor with non-degenerate bands with extrema at $k=0$, which was outlined in Chapter 1. Section 3.1.2 describes the single particle states that occur in Si. This is followed by an explaination of the shell model in Sec. 3.1.3.

3.1.2 Donor and acceptor single particle states

A description of the single particle donor states in Si is complicated by the fact that the conduction band minimum is not located at the zone center. As a consequence of this, and of the symmetry of the crystal, there are six equivalent minima of the conduction band. This means that the 1S ground state becomes six-fold degenerate (without including spin, which does not have to be explicitly included because there are no large spin dependent terms in the Hamiltonian). Linear combinations of these six states are split into three different energy levels by the impurity potential.[17] The resulting groups of degenerate states can be labelled according to the way they transform under the point group of the crystal. The ground state is one-fold degenerate (not including spin)and transforms into itself according to a one dimensional representation of the tetrahedral point group, Γ_1.[18] The next set of states transforms according to a three dimensional representation of the group, Γ_5. Finally the remaining two states transform according to the Γ_3 irreducible representation. The splitting between the Γ_1 and Γ_5 states is 11.9 meV, and between the Γ_5 and Γ_3 is 1.4 meV for phosphorous.[19]

The maximum of the valence band, while at $k=0$, is four-fold degenerate in silicon, including spin. Here, spin is included because spin-orbit terms

are important at the top of the valence band.[20] The lowest energy bound state in this case still has a 1S envelope function, but the quantum number describing the way in which the wave function transforms in the crystal field is now Γ_8, the label of a four dimensional irreducible representation of the tetrahedral double group.

3.1.3 Shell model of multiple bound exciton complexes

The shell model[15,16] makes predictions about the nature of the multiple bound exciton states. The model also predicts which transitions among these levels account for the spectroscopy.

The ground state of the bound exciton is constructed, within this model, by placing two of the electrons in Γ_1 states (this is allowed by the Pauli exclusion principle because of the two spin states implicitly included), and by placing the hole in a Γ_8 state. This is shown in Fig. 3.2. The first excited state of the bound exciton is formed by replacing one of the Γ_1 electrons by a Γ_3 or Γ_5 electron. The energies of the Γ_3 and Γ_5 states are fairly close and the model does not differentiate between them. The two exciton complex adds one electron and one hole to this description. The ground state is constructed by adding one electron in a Γ_3 or Γ_5 state to the ground state of the single bound exciton, and one hole in a Γ_8 state. The first excited state of this complex is then made by promoting one of the Γ_1 electrons to a Γ_3 or Γ_5 electron. The larger complexes are constructed in a similar fashion, placing as many of the particles as possible in the lowest energy single particle states for the ground state of a given complex, and making the excited state of a complex by promoting one of the electrons.

The shell model makes some assumptions about expected splittings of a single level and about the way various levels of the multiparticle states mix.

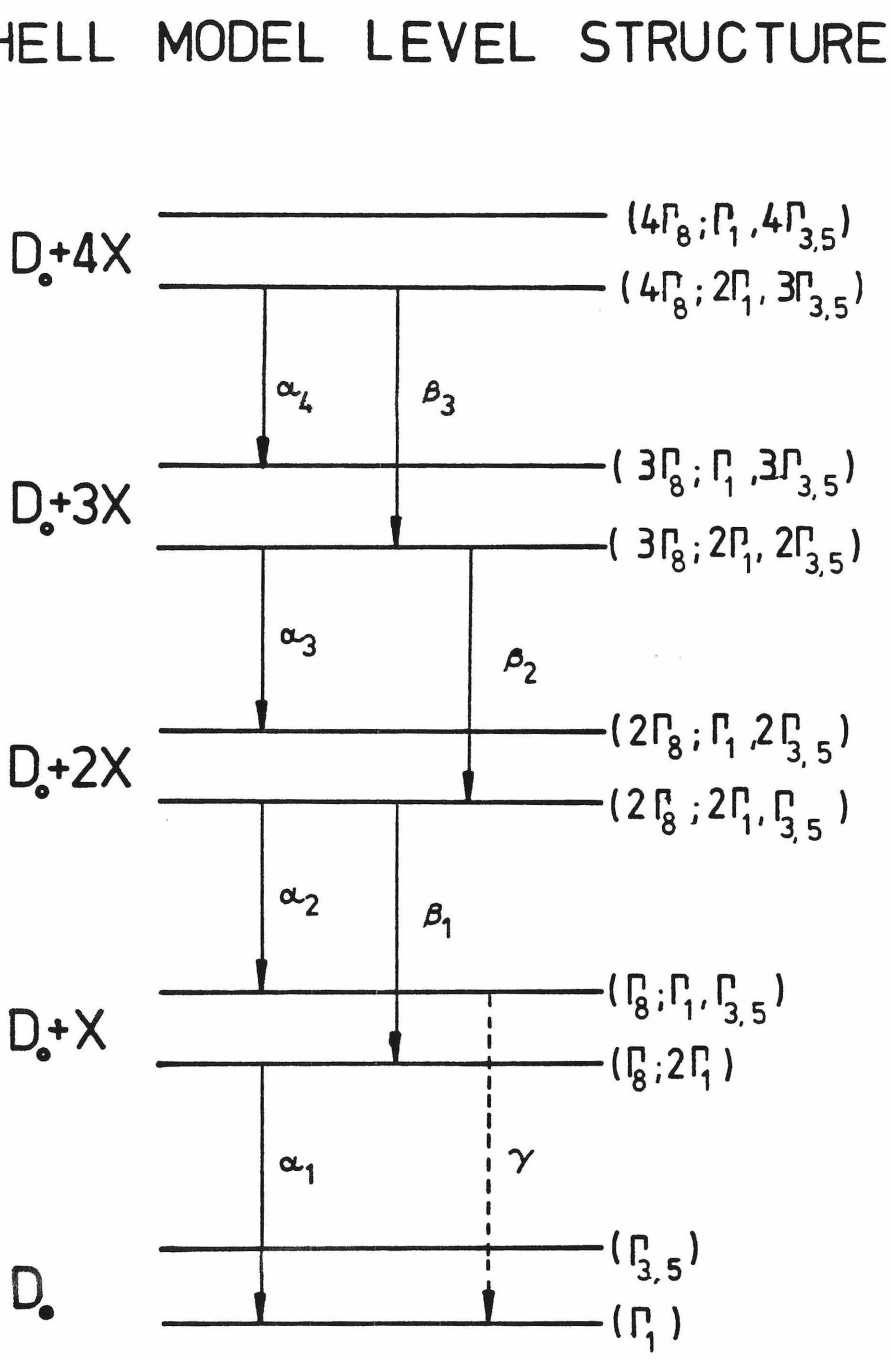

Figure 3.2: The shell model level structure for donors in Si. The labels for the levels and the transitions are taken from Ref. 15. D_o indicates the neutral donor, D_o + nX indicates a donor with n excitons bound to it. The single particle configurations are given at the right.

For example, the states formed by the product of a Γ_8 hole and a Γ_3 electron could split into as many as three different levels, but the shell model assumes such splittings are small. Also, in order for the single particle quantum numbers to be reasonable descriptions of the multiparticle states, mixing of other single particle states whose product has the same overall symmetry must be small.

The shell model interpretation has had some successes in explaining the spectroscopic data.[21] It is assumed that the alpha series of transitions occur when a Γ_1 electron recombines with a Γ_8 hole, and the beta series when a Γ_3 electron recombines with the hole. This is shown in Fig. 3.2, where the verticle arrows indicate radiative transitions. In the shell model, the energy difference between the α_2 and β_1 line is the difference between the ground and excited state of the single bound exciton. If this is true, the transition between the excited state of the bound exciton and the ground state of the donor (labelled γ in the diagram), should be displaced from the α_1 transition by this same energy difference. The γ transition is observed, and at the predicted energy, in high temperature luminescence.[9] However, not all the data agree with the predictions of the shell model. For example, the systematics of the splittings for different donors is not what is qualitatively expected.[13] Further, stress data show that two of the β series (β_1 and β_2) split into more lines than expected on the basis of the shell model.[12,13]

3.1.4 Experimental test of a shell model prediction

In order to resolve the controversy over the origin of the multiple bound exciton lines, further tests were needed. As a check on the shell model level structure, lifetime measurements of some of these lines were made. In the shell model, the α_n line should have the same initial state as the β_{n-1} line, which is the ground

state of a complex binding n excitons. This prediction can be tested by examining the decay characteristics of these lines since lines with the same initial state should exhibit identical decays. Different decay characteristics would definitively rule out the shell model. Sauer, et al[9] have attempted to test this hypothesis by measuring the decay in the transverse-optical (TO) phonon-assisted transitions. They found that the decays of the α_3 and β_2 lines differ, as do the α_4 and β_3. Hence, they conclude that the shell model interpretation is invalid.

Close inspection of the TO-phonon spectrum, however, shows that the measurement is not completely straightforward. As shown in the upper spectrum in Fig. 3.1, the lines in the no-phonon spectrum are sharp and distinct with little background, making possible an accurate measurement of the decay of a given line. This is in contrast to the TO-phonon spectrum, in which there are more lines, the lines are broader, and the lines are superimposed on a background. As pointed out by Thewalt,[10] the determination of the decay characteristics using the TO phonon-assisted transitions may have been confused by the overlap of lines and background with different decay characteristics.

To attempt to determine which lines could have the same initial states, we have made transient measurements on lightly doped Si:P samples and analyzed the data taking careful account of the overlap of lines. The data were recorded to greater accuracy and to longer times than than those recorded in Ref. 9. The decay of the α_1, α_2, α_3, and α_4 lines were measured in the no-phonon replica. The decays of the β_1 , β_2, and β_3 were measured in the TO-phonon replica since they do not occur in the no-phonon region. The decay of the β lines was compared with various combinations of the decays of the α lines as observed in the no-phonon transition to assess which lines could have the same initial states.

3.1.5 Outline of chapter

The remainder of this chapter is organized in the following way: Section 3.2 describes the experimental setup and the steps taken to insure proper treatment of the dark count and response of the photon counting equipment. The experimental results are presented in Sec. 3.3. Section 3.4 includes the results from fitting the decay of the β lines to various combinations of the α lines. Section 3.5 contains our conclusions based on the quality of the various fits, and discussion about its relevance to the shell model and more recent theoretical work.

3.2 EXPERIMENT

3.2.1 Sample preparation

The transient measurements were made on a 2 mm thick wafer of high-purity Wacker silicon, transmutation doped with phosphorous to the 1.5×10^{14} cm^{-3} level. The sample was prepared in this way to obtain a very low boron to phosphorous ratio, because boron bound exciton luminescence was an undesirable background. Hall measurements on this sample indicated N_A-N_D was $\sim 2\times10^{11}$ cm^{-3} before doping. Luminescence measurements on the undoped sample did not show a detectable phosphorous bound exciton line, but did show some boron bound-exciton luminescence.[22] The relationship between bound exciton luminescence intensity and concentration[23] indicated that the sample was not closely compensated and therefore was very low in boron. The sample was then phosphorous doped by neutron irradiation. Ordinary silicon contains about 3% ^{30}Si, and these atoms capture neutrons to become ^{31}Si. This isotope of silicon is not stable and beta decays, with a half life of 2.6 hours, to form ^{31}P, the stable isotope of phosphorous. The sample was then annealed to remove the radiation damage. The final result was a sample with a very low boron to

phosphorous ratio, but which still maintained a phosphorus content low enough to avoid concentration broadening of the luminescence.

3.2.2 Generation and detection of luminescence

The system used to generate the luminescence signal was fairly straightforward, and will be described briefly. It is illustrated in Fig. 3.3, which is a schematic of the entire experimental apparatus. The sample and a GaAs diode laser, used to pump the sample, were immersed in liquid He at 4.2 K in a Janis research dewar. The laser light (centered at 8500 Å) was directed onto the center of a polished and etched surface of the sample, with a spot size of about 1 mm^2. The peak excitation power density was varied between ~ 8 W cm^{-2} and ~ 70 W cm^{-2} by adjusting the amplitude of the current pulse driving the laser. The current pulses were of 0.5 μsec duration 5 μsec apart, and were provided by a Systron-Donner 114A pulse generator.

The RCA SG-2004 laser diodes are very convenient sources of pulsed excitation for this experiment, but are not well documented elsewhere because RCA's literature gives specifications only at room temperature. The resistance changes drastically at low temperatures, and consequently the maximum current specifications change. Maximum operating conditions to prevent destruction of the diodes were: current times duty factor less than 16 amp-percent (limits on the average power dissipated), and current times pulse length less than 8 amp-μsec (limits on the instantaneous power).[22] The pulser used to drive the diodes was chosen because it was able to provide up to about 2 amp at 50 volt, which was necessary to drive the diodes at their maximum power, while the fall time of its pulses was low enough to allow laser fall times with exponential decays of about 5 nsec. The peak output of the laser at 2 amp and at 4.2 K was approximately 1 W. A small fraction of the lasers have a luminescence back-

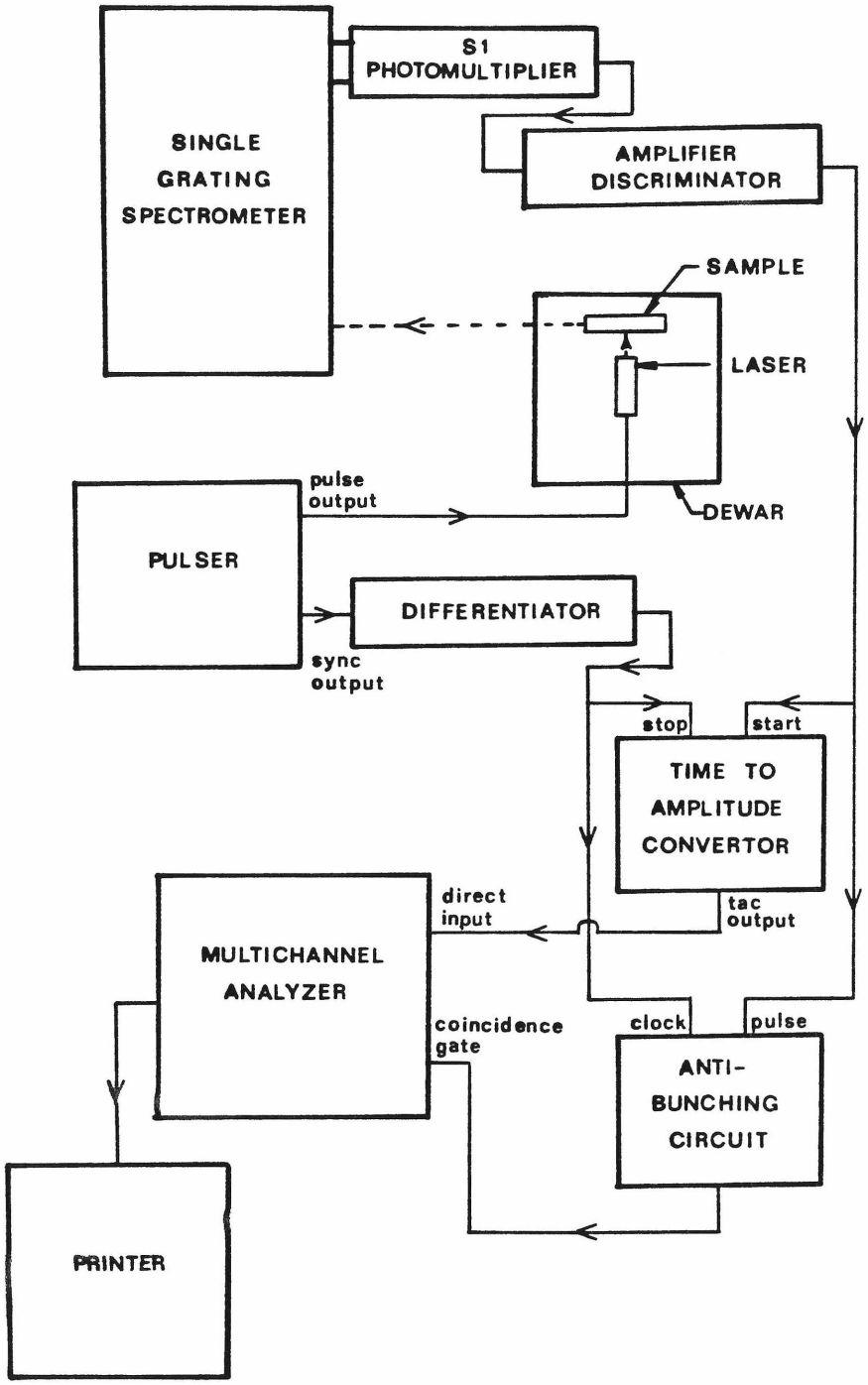

Figure 3.3: Schematic of the apparatus used in the experiment.

ground at about 1 μm in wavelength, making them unsuitable for work in Si. One disadvantage of using the diode lasers as pulsed sources was that the output power changed with temperature for a given current, adding some uncertainty in the pump power in an experiment which measured the temperature dependence of decay rates. This was not a problem in these experiments, as all the data were taken at 4.2 K.

The luminescence from the sample was analyzed and detected with a spectrometer-photomultipier system. This is also shown as part of Fig. 3.3. Luminescence from the edge of the sample was focused onto the the aperture of a Spex 1269 spectrometer. This sample geometry (pumping the flat surface of the wafer, and pointing the edge toward the spectrometer) was chosen because it maximized the signal. The resolution of the spectrometer was 3.5 Å with the slit width and grating used for the experiment. A visible light filter placed in front of the aperture reduced stray light from the laser and the instrument-rack lamps. A liquid-nitrogen cooled photomultiplier tube (with S1 response) detected the luminescence passing through the spectrometer. Finally, the output of the photomultiplier tube was fed into a PAR 1120 amplifier discriminator.

3.2.3 Timing and counting of photon pulses

The luminescence signal leaving the amplifier discriminator was further processed by a system that measured and stored the time with respect to the laser pulse that the signal arrived. This system is illustrated in Fig. 3.3. Photon pulses leaving the amplifier-discriminator (negative going, 15 nsec long pulses) were used to start an Ortec model 467 time to amplitude converter. Some fixed time after the laser pulse occurred, the pulser sent out a pulse on the synchronous output. This pulse was differentiated and rectified to provide a negative going timing pulse about 20 nsec wide, which served as the clock pulse for the

experiment. This pulse was used to stop the time to amplitude converter. The output of the time to amplitude converter was then fed into an Nuclear Data ND60 multichannel analyzer, which converted the pulse height into the corresponding channel number. The resulting spectrum on the multichannel analyzer displayed intensity of counts as a function of time before the sync pulse from the pulser. Additional electronics (the anti-bunching circuit) allowed the multichannel analyzer to process the time to amplitude converter output if and only if one photon was detected during the timing interval associated with a given laser pulse. The system could measure the time of arrival of only the first of the photons, and storing its time while ignoring that of the second would bias the data. The circuit used for this purpose could resolve pulses as close together as 50 nsec.

3.2.4 Discussion of system response

The response of the photomultiplier tube was an important factor in the experiment, and deserves further discussion. One non-ideal feature of the tube that affected our results was dark count. The dark count gave a uniform (in time) background of approximately 6 counts sec^{-1} to all the data. Subtraction of the dark count was, therefore, a very straightforward procedure.

The second non-ideal feature of the tube was after pulsing, which was also a source of background in the transient measurements. Unlike dark count, after pulsing is not uniform in time. After pulsing is the detection of a spurious pulse up to many microseconds after the first, real pulse is detected in the photomultiplier tube. The process seems to be associated with the movement of ions back down the tube after being created by the electron cascade. The after-pulsing distribution was measured by two methods to determine whether the nonuniformity in time of the after pulsing affected the transient measurements.

The first method was a direct measurement of the pulse pair distribution. The time to pulse height converter was used to measure the time difference between successive pulses during uniform illumination of the photomultiplier tube. If no after pulsing occurs, the measured distribution should be an exponential with lifetime equal to 1/R (~ 2 msec for this measurements), where R is the count rate. The measured distribution was much steeper than this, however, and the initial 5 μsec of the distribution decayed with an exponential decay time of 3.2 μsec. The transient experiment, however, was not sensitive to this initial part of the after pulsing distribution, because of system dead time. The later part of the after-pulsing distribution dropped off less steeply than 3.2 μsec, but the distribution could not be measured accurately because of low signal to noise. Also, the pulse pair distribution may not give the entire after-pulsing distribution because the pair distribution ignores correlations between triples of pulses.

A second, indirect method, was used which measured the entire after-pulsing distribution in the region of time where it affected the experiment. This was done by looking at the actual data. The transient curves stored on the multichannel analyzer showed background both before the laser pulse went on and after luminescence died away. Background was calculated by averaging over 50 channels (~ 350 nsec) in each of the regions. These regions occurred at different times with respect to the initial laser pulse, and so sampled different parts of the after-pulsing distribution. However, the intensity of the background in each region agreed to within statistical error (except for long-lived lines where the signal did not die away fast enough to allow the measurement to be made). This indicated that over the time interval of interest in the experiment, the after-pulsing distribution was uniform enough to be treated at a flat background. Therefore, the after pulsing could be taken into account merely by subtracting

the average background from each channel of the multichannel analyzer.

Several other possible sources of error introduced by the timing and counting equipment were considered. First, the difference in time between the pulse to the laser and the sync output of the pulser varies somewhat from pulse to pulse. For the delays used in the experiment, this random jitter was less than 10 nsec, and was neglected. The time to channel number conversion was calibrated by measuring the time difference between the sync output and pulse output of the pulser with both this measurement system and a Systron-Donner 6361 frequency counter (in a mode which measured the time difference between inputs to 10 nsec). Finally, the application of the coincidence pulse from the anti-bunching circuit to the ND60 occasionally resulted in two channel "glitches" in the accumulated spectra, in which one channel would have too many counts, and the adjacent channel too few. Apparently, the analog-to-digital converter was not sufficiently isolated from the coincidence gate. However, the rest of the amplitudes were converted correctly, so this had no effect on the results. This problem might be eliminated altogether by using an anticoincidence requirement for recording a pulse rather than a coincidence requirement.

3.3 EXPERIMENTAL DATA

Using the system described above, various transients were measured. The lines measured in this way include the no-phonon α-series, and the TO-phonon β_1, β_2, and β_3. Pump power dependences of several lines were also investigated. Fig. 3.4 illustrates two factors that determine, in part, the resolution and accuracy of the measurements. The first is the laser decay, which is quite fast in comparison to the luminescence decays. The second is the scatter in the data points. The size of the error bars (shown for several points) primarily reflects statistical uncertainty in the counts per channel before subtracting dark count and after

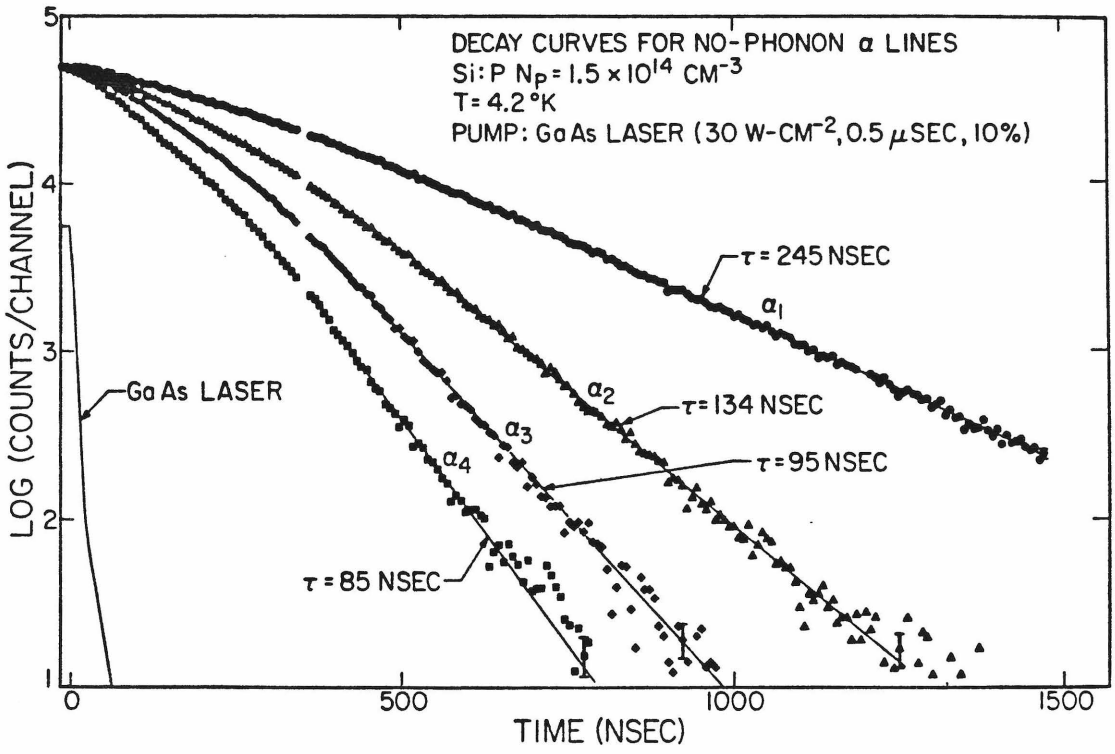

Figure 3.4: The logarithm to the base ten of the transient decay of the α_1, α_2, α_3, and α_4 lines in the no-phonon replica. The points are the experimental data. The solid lines are straight-line fits to the decays at long times. The decay times given are obtained by converting the slopes of these lines to base e. The solid line labeled GaAs laser is the experimental decay for the laser used in the experiment.

pulsing.

3.3.1 Decay of the alpha lines in the no-phonon replica

Decays of the α_{1-4}, each at the same pump power, are shown in Fig. 3.4. The curves are exponential except in the earlier region, just after the laser shuts off. Decay times, derived from the later exponential parts of the curve, are 245 nsec for α_1, 134 nsec for α_2, 95 nsec for α_3, and 85 nsec for α_4. The error bars are ± 10 nsec for the α_1 time, and ± 5 for the other three. α_5 and α_6 show similar decays, except the curves break to slower decays at long times. This break is probably due to the presence of low intensity, long lived background lines, which show up in the α_5 and α_6 decays because both these lines are themselves low in intensity.

The rounding seen in all the a lines at early times increases with pump power, as illustrated for α_3 in Fig. 3.5. The decays all become exponential eventually, with the same lifetime, but for the highest pump power the curve does not become straight until over 600 nsec after the laser has shut off. This initial rounding would lengthen "decay times" derived by fitting an exponential decay to earlier segments of the curves, and may explain why our results differ from the decay times quoted by Sauer.[9]

3.3.2 Decay of the beta lines in the TO-phonon replica

Figures 3.6, 3.7, and 3.8 show the decays for β_1, β_2, and β_3, respectively. In each figure, the points show the log of the number of counts/channel vs channel number (or time). Only one out of every three data points is plotted, to make the lines plotted on the figure visible. All the data collected were used for the analysis, however.) The lines are "fits" made by adding other transient curves together, which will be discussed later. The lines are offset, and data repeated, to make comparison of the various fits easier.

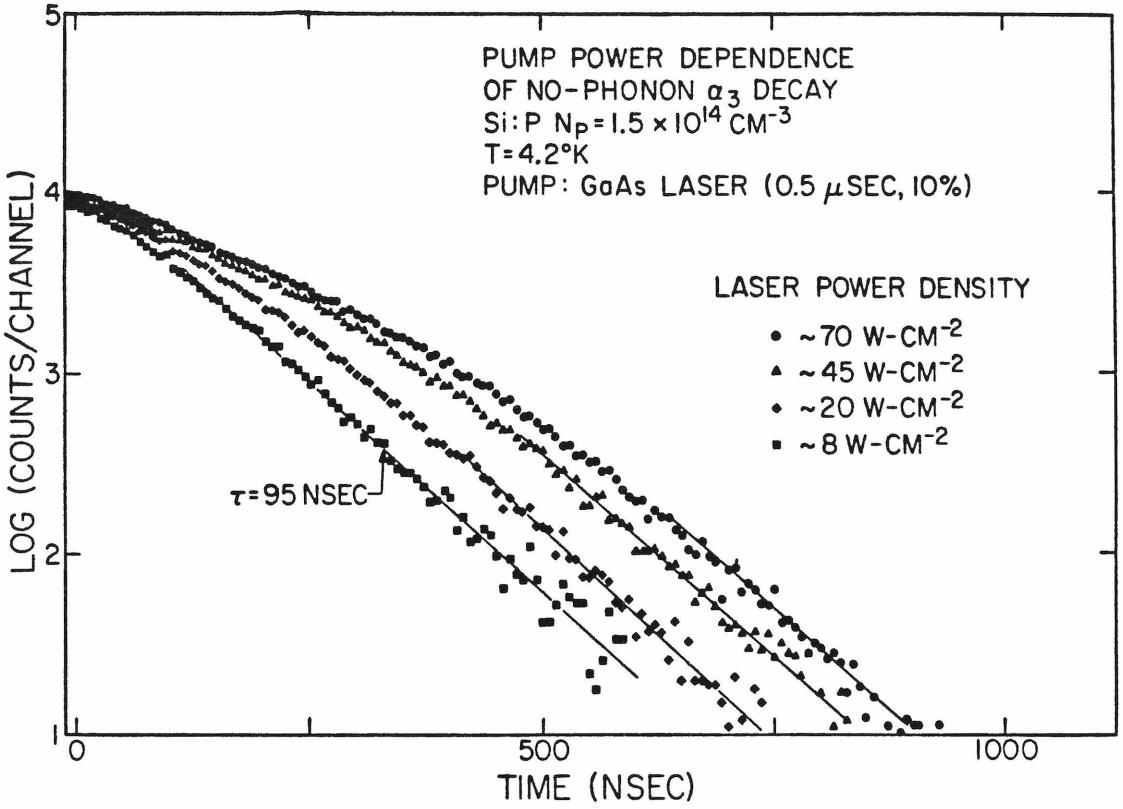

Figure 3.5: The logarithm to the base ten of the transient decay of the α_3 line in the no-phonon transition for a number of different laser pump power densities. The straight lines all have a slope appropriate to a 95 nsec exponential decay time.

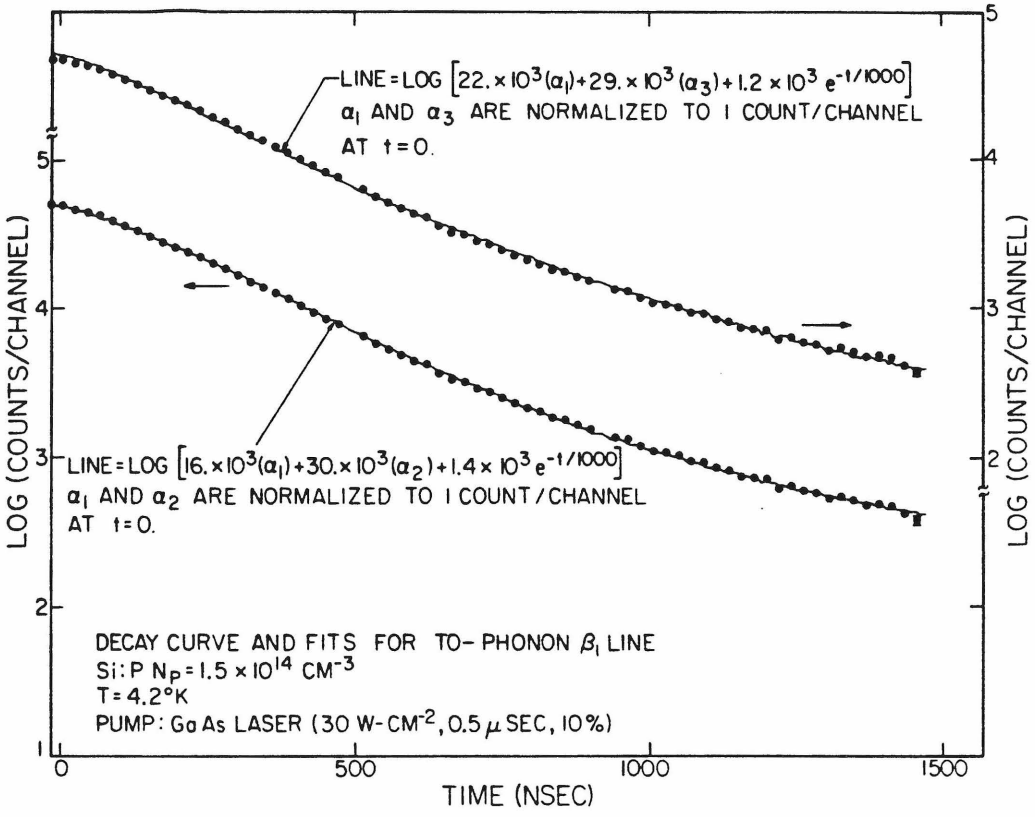

Figure 3.6: The logarithm to the base ten of the decay of the β_1 line. The points are the experimental data which have been plotted twice with the upper set referring to the axis on the right and the lower set referring to the axis on the left. The solid lines are the results of fitting the experimental data to the indicated combinations of other lines.

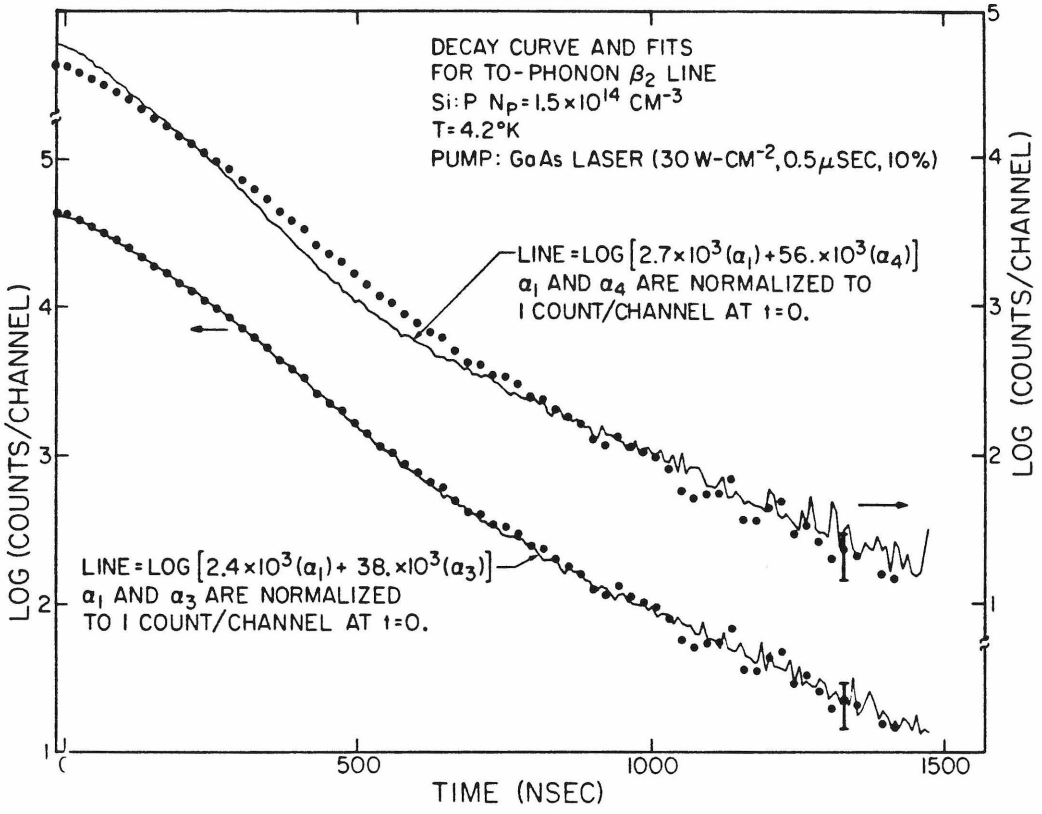

Figure 3.7: The logarithm to the base ten of the transient decay of the β_2 line. The points are the experimental data which have been plotted twice with the upper set referring to the axis on the right and the lower set referring to the axis on the left. The solid lines are the results of fitting the experimental data to the indicated combinations of the decay of other lines.

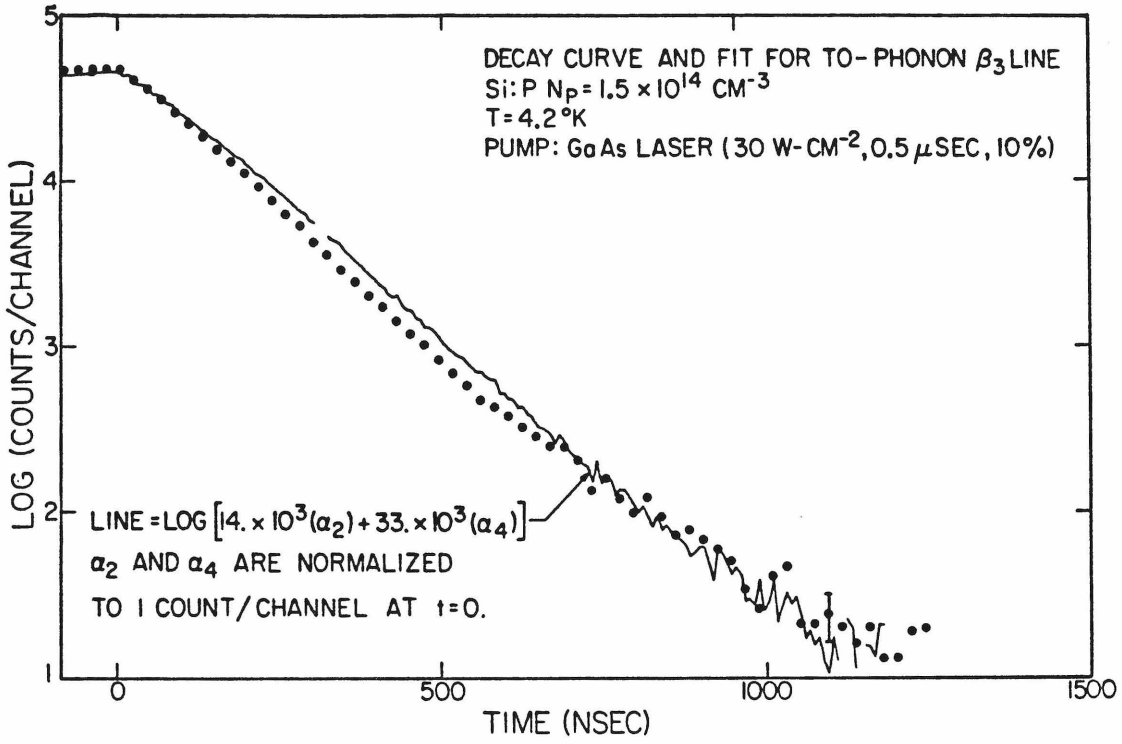

Figure 3.8: The logarithm to the base ten of the transient decay of the β_3 line. The points are the experimental data. The solid line is the result of fitting the experimental data to the indicated combinations of the decay of other lines.

The decay curve for β_1 (Fig. 3.6) shows three different regions. The first, just after the laser shuts off at $t=0$, shows a rounding discussed earlier. The fairly straight region from about 600 nsec to 1200 nsec decays somewhat faster than that of the phosphorus bound exciton, clearly indicating that the β_1 line, without the α_1 and other lines underneath it, has a decay time faster than 245 nsec. The last segment of the curve shows a definite break to a decay time much slower than that of phosphorus bound exciton, and is due to the boron bound exciton, with a lifetime of about 1000 nsec.[24]

The decay curve for β_2 (Fig. 3.7) also has three different regions. First, it shows the same rounded part as for all the other curves. The second part, from about 800 nsec to 1200 nsec, is again almost straight. The last segment of the curve, which breaks to a slower decay time, is due to the tail of a longer lived line that overlaps β_2. This is probably either the phosphorus bound exciton, or a boron exciton-complex line. The initial part of this curve clearly decays faster than α_2 even without subtracting out the longer lived tail under the β_2 line.

The β_3 curve is shown in Fig. 3.8. The rounding of the initial part of the curve is not as apparent here as it was for β_1 and β_2, but it is still present. The decay is almost exponential until ~500 nsec after the laser shuts off, when the curve shows a definite break to a longer decay time. Since β_3 sits on the shoulder of the TO-phonon α_2 line, the α_2 line causes at least part of the break. However, there is also a boron exciton-complex line at almost the same wavelength as α_2,[3] which could also contribute to the break. The initial 200 or 300 nsec segment of the β_3 decay curve clearly decays faster than the no-phonon α_3, even before subtracting out the longer lived component under the β_3 line. The initial part of the β_3 also decays very slightly faster than the no-phonon α_4 line.

3.4 ANALYSIS OF DECAYS

The method of analysis differed for the α- and β-series of decay curves. No other lines of appreciable intensity overlap the no-phonon α_1, α_2, α_3, or α_4, and their decays reflect this by showing exponential behavior after some initial rounding. Therefore, the straightforward analysis of these transients, interpreting them each as the decay of a single luminescence line, is fairly reliable. This is not the case for the β-series of lines. The β-series is not visible in the no-phonon spectrum, and the TO-phonon replica of each of the three β-series lines overlaps an α-series line. Also, the presence of boron bound-exciton lines and the possible presence of a broad background in the TO-phonon spectrum further complicates the decays of the β-lines. Hence, the straightforward analysis used for the α lines is not appropriate for the β lines.

To deal with the background and overlaps for the β_1, β_2, and β_3, various combinations of other decay curves were added together in an attempt to reproduce the particular β decay under consideration. The actual data were used in these composite curves, because the rounding exhibited by all the decays ruled out fitting the β curves analytically as the sum of exponentials. The amplitude of each component in the composite curve was determined by a nonlinear least-squares method. In plotting the resulting fit (see Figs. 6, 7, and 8) continuous curves were used to distinguish the fit from the β-decay data points.

3.4.1 Analysis of the beta one decay

The extraneous components of the β_1 decay were taken to come from the α_1 line, since the β_1 sits on the shoulder of the TO bound exciton line, and from the boron bound exciton line, since this line is known to sit at approximately the same wavelength as β_1. The decay of the β_1 was compared with both the α_2 and α_3 lines. In each case, the extraneous components were added to the α data,

and the result compared to β_1. More specifically, if $\beta_1(I)$, $\alpha_1(I)$, etc., are the number of counts (minus dark count and afterpulsing) in channel I on the MCA (corresponding to intensity of luminescence light detected during a time window at time $t(I)$) then the function

$$\sum_I \left[\log\beta_1(I) - \log[a\,\alpha_1(I) + b\,\alpha_i(I) + c e^{-t(I)/1000\text{nsec}}]\right]^2. \qquad (3.1)$$

was minimized by varying the parameters a, b, and c. An analytic form was chosen to represent the effect of the boron, since the boron bound exciton transient curve itself could not be obtained for this sample. Fig. 6 shows the fits. The upper curve is the result using $\alpha_i = \alpha_3$ in Eq. 3.1. The points are the log of the β_1 data, the line is the log of the sum of parts. The fit looks fairly close; it may, however, decay too steeply at the beginning to fit the data. The second curve is the result for i=2. This fit is slightly better than the previous one, as indicated by the error criterion of the least-squares fitting procedure. However, the similarity of the two different fits indicates that this is not a particularly sensitive test for the β_1 decay time.

3.4.2 Analysis of the beta two decay

The extraneous component of the β_2 transient was taken to come from the tail of the α_1. The function to be minimized for the fit to this decay was

$$\sum_I \left[\log\beta_2(I) - \log[a\,\alpha_1(I) + b\,\alpha_i(I)]\right]^2 \qquad (3.2)$$

done by varying a and b. Figure 7 shows the results. The points are the log of the β_2 data, the line the log of the fit, drawn as a continuous curve. The top plot in the figure is for i=4 in Eq. 3.2, clearly a bad fit. The bottom plot is for i=3, and seems to be an adequate fit. However, it is not clear that α_1 is the only line that could affect the β_2 decay. A boron multiple bound exciton line sits between

the β_2 and α_1, as does the LO-phonon replica of α_2.

3.4.3 Analysis of the beta three decay

We attempted to fit the β_3-decay to the α_4-decay. Overlap from the α_2-line was included by adding the α_2 transient to the α_4 transient, the coefficients of each determined by minimizing

$$\sum_I \left[\log\beta_3(I) - \log[a\,\alpha_2(I) + b\,\alpha_4(I)] \right]^2.$$

This fit, shown as a solid line in Fig. 8, is not a particularly good one. As pointed out earlier, β_3 decays slightly faster than the no-phonon α_4 line at early times even before subtracting out the longer lived component under β_3. However, this still does not rule out the possibility that β_3 decays like α_4, because the broad background found in the TO-phonon spectrum has not been taken into account. A comparison of the transient curves of the no-phonon and TO-phonon replicas of the α_3 line indicates the broad background decays faster than α_3, because the TO-phonon replica of α_3 decays slightly faster at early times than its no-phonon counterpart. If this same background were present under the β_3 line, it alone could cause the fitting procedure to fail, because the background was not included in the composite curve.

3.5 CONCLUSIONS

3.5.1 Summary of results

The data and analysis presented above allow us to place limits on the decay of the β-series lines, but do not allow us to conclude unambiguously whether or not a given β decay is identical to any of the α decays. The β_1 line decays faster than α_1, but its decay may be like that of either α_2 or α_3. The error criterion of the

fitting procedure indicates α_2 provides a better fit, but the fitting procedure is not a very sensitive test of the β_1 decay. Further, our uncertainly in the precise form of the decay of the boron bound exciton, particularly at early times, is comparable to the difference in the fit using α_2 and α_3. The limits on the β_2 decay are better defined. The β_2 decays faster than α_2, but more slowly than α_4. The fit with the α_3 decay works well. Finally the β_3 decays more rapidly than the α_3. The fit to the α_4 is not very good; however, the differences could be due to unaccounted for background.

3.5.2 Significance of results

These results do not settle conclusively the question of the validity of the shell model, although the results are consistent with the prediction that the α_m and β_{m-1} lines have the same initial state. This conclusion, however, was very timely because of other work[9] that came to different (and erroneous) conclusions about the lifetimes. The lifetime measurements, instead of conclusively ruling out the level structure predicted by the shell model, indicate that it might be correct.

Much work remained to be done to establish the separate question about the nature of the states that make up the level structure, however. An extensive theory of the bound multi-exciton complexes was formulated some time after these lifetime measurements.[25,26]. This theoretical work demonstrates that certain of the shell model assumptions are essentially correct. In particular, it shows that the splittings within a given single particle configuration and the degree of mixing between different configurations are fairly small, at least for substitutional donors like phosphorous. This theory goes well beyond the shell model, however, in that it correctly predicts ground to excited state separations for the different complexes, and allows a quantitative

evaluation of the assumptions incorporated in the model.

REFERENCES

1. A. S. Kaminskii, Y. E. Pokrovskii, and N. V. Alkeev, Zh. E.T.F. **59**, 1937 (1970).
2. R. Sauer, Phys. Rev. Lett. **31**, 376 (1973).
3. K. Kosai and M. Gershenzon, Phys. Rev. B **9**, 723 (1974).
4. P. J. Dean, D. Herbert, D. Bimberg, and W. J. Choyke, Phys. Rev. Lett. **37**, 1635 (1976).
5. M. L. W. Thewalt, Phys. Rev. Lett. **38**, 521 (1977).
6. S. A. Lyon, D. L. Smith, and T. C. McGill, Phys. Rev. B **17**, 2620 (1978).
7. M. L. W. Thewalt, Solid State Commum. **21**, 937 (1977).
8. M. L. W. Thewalt, Can. J. Phys. **55**, 1463 (1977).
9. R. Sauer, W. Schmid, and J. Weber, Solid State Commun. **24**, 507 (1977)
10. M. L. W. Thewalt, Solid State Commun. **25**, 513 (1978).
11. S. A. Lyon, D. L. Smith, T. C. McGill, Phys. Rev. Lett. **41**, 56 (1978).
12. M. L. W. Thewalt and J. A. Rostworowski, Phys. Rev. Lett. **41**, 808, (1978).
13. K. R. Elliott and T. C. McGill, Solid State Commun. **28**, 491 (1978).
14. T. N. Morgan, in Proceedings of XIII International Conference on the Physics of Semiconductors, edited by (Marver, Rome, 1976) p. 825.
15. G. Kirczenow, Solid State Commun. **21**, 713 (1977).
16. G. Kirczenow, Can. J. Phys. **55**, 1787 (1977).
17. See, for example, F. Bassini and G. Pastore Parravicini, *Electronic States and Optical Transitions in Solids* (Pergamon Press, Oxford, 1975), Chap.7, Sec.3.
18. The notation is that used in G. F. Koster, J. O. Dimmick, R. G. Wheeler, and H. Statz, *Properties of the Thirty-two Point Groups* (Massachusetts Institute of

Technology Press, Cambridge, Mass., 1963).

19. A. L. Aggarwal, Solid State Commun. **2**, 163 (1964).

20. A. Baldereschi, N. O. Lipari, Phys. Rev. B **8**, 2697, (1973).

21. M. L. W. Thewalt, to be published in Proceedings of XIV International Conference on the Physics of Semiconductors.

22. S. A. Lyon (unpublished).

23. M. Tajima, Appl. Phys. Lett. **32**, 719 (1978).

24. S. A. Lyon, G. C. Osbourn, D. L. Smith, and T. C. McGill, Solid State Commun. **23**, 425 (1977).

25. Y. C. Chang, and T. C. McGill, Phys. Rev. Lett. **45**, 471 (1980).

26. Y. C. Chang, and T. C. McGill, to be published in Phys. Rev. B.

CHAPTER 4

SELECTIVE EXCITATION LUMINESCENCE IN BULK-GROWN GaAs

4.1 INTRODUCTION

4.1.1 Motivation for work

Luminescence from semiconductors can provide insight on the physics of semiconductors, but can also be a very important diagnostic tool.[1] The energy of impurity related luminescence in many cases can reveal the identity of the impurity. The technique, however, seems most useful for samples of light to moderate impurity concentrations.[2] Much higher pump densities must be used to get comparable signals in heavily doped samples because the deep centers can capture a large fraction of the free carriers. Furthermore, as impurity concentrations are increased, lines broaden and, in the case of donor-acceptor luminescence, peaks shift in energy.[2] Recent work in Si[3] indicates that transfer of excitation can occur, when excitons, on the shallow acceptor boron, tunnel to the deeper center indium. At sufficiently high indium concentrations, no boron bound exciton luminescence can be detected.[3] These difficulties make luminescence results for heavily doped samples more ambiguous than for lightly doped samples.

Bulk-grown GaAs is an example of a technologically important material for which the impurity concentrations can be very high. It is often used as a high resistivity substrate material for devices.[4] At the current level of material growth, high resistivity material is achieved by placing a sufficient number of deep levels in the material to compensate the shallow levels that are always inadvertently present.[4] The resulting high impurity concentration makes interpretation of luminescence experiments difficult.

This is in contrast to the case of high quality epitaxial GaAs, where the identification of shallow acceptors by the use of straightforward photoluminescence is fairly well advanced.[2] Two different luminescence lines have been used

to identify shallow acceptors in epitaxial GaAs. The first is bound-exciton recombination luminescence in which the remaining hole is left in a hydrogenic 2S state, called the two-hole transition.[2,5,6] The energy difference between this line and the principal bound-exciton line yields the 1S to 2S energy difference for the acceptor. This difference is characteristic of the particular acceptor because the 1S energy of the hole is sufficiently perturbed by the ionic core to show a significant central-cell shift, while the 2S state shows a much smaller shift. A second method which can be used to identify the shallow acceptors in some cases is to measure the position of the donor-acceptor or free-electron to bound-hole luminescence bands.[1,6]

The higher impurity concentration in the bulk grown material leads to line broadening and lower luminescence intensities, so that the techniques that were useful on the epitaxial GaAs are no longer as useful.[2] In particular, the two-hole transition luminescence is seen only on the highest quality epitaxial samples.[6] As mentioned above, the position of donor-acceptor bands can be shifted by high impurity concentrations.[2] Therefore, different methods must be used to identify the common shallow acceptors in bulk-grown GaAs than are used in epitaxial GaAs.

Selective excitation luminescence, a form of excitation spectroscopy in which excited states of the acceptor are selectively populated, is capable of providing unambiguous identification of acceptors even in bulk-grown material with very little luminescence intensity. This technique has been used successfully in bulk-grown InP,[7,8] and also has been used in ZnTe[9] and ZnSe.[9,10]

4.1.2 Results of this work

Luminescence spectra with above band gap excitation were taken on two bulk-grown GaAs samples, one semi-insulating and one p-type. The semi-insulating

sample had a very weak luminescence signal from the near band gap donor-acceptor lines, making identification of the acceptor by the position of this band difficult. The low luminescence yield was apparently due to a large concentration of a deep level, as indicated by the presence of a very high intensity luminescence band with a low photon energy.

We were able to conclusively identify the principal acceptor in both bulk-grown samples, by the use of selective excitation luminescence. Neither of the samples were intentionally doped with shallow acceptors. We have identified the acceptor as Zn for the first sample, and C for the second, as will be shown below. The identification of the acceptor in the p-type sample was verified by Raman scattering by the occupied acceptors. In making these identifications, we have shown selective excitation spectroscopy to be a useful probe of impurities and impurity levels in bulk-grown GaAs, where high impurity concentrations make other methods less useful.

4.1.3 Outline of chapter

The technique of selective excitation luminescence used to identify the acceptors in the bulk grown samples will be discussed in Sec. 4.2. Section 4.3 will cover the experimental details. The results of the experiments and their interpretation will be covered in Sec. 4.4. The results will be summarized and the significance of the results will be discussed in the final section, Sec. 4.5.

4.2 SELECTIVE EXCITATION LUMINESCENCE TECHNIQUE

4.2.1 Sequence of transitions

In selective excitation luminescence, [9,10] a tunable, below band gap laser is used to create an electron on a donor and a hole on an adjacent acceptor, with the hole in an excited state. While pairs should be produced with the electron in an

excited state also, lines due to this process are not observed. Therefore, they are not included in this description, although reasons for their absence from the spectra will be discussed below. The energy required to create the donor-acceptor pair is $\hbar\omega_{laser} = E_g - E_A^* - E_D + e^2/\varepsilon R$, where E_g is the band gap, E_A^* the energy of the excited hole with respect to the valence band, E_D the energy of the electron with respect to the conduction band, and $e^2/\varepsilon R$ is the coulomb attraction of the ionized centers at distance R from one another. This is illustrated in Fig. 4.1, where the energy of the occupied pair is plotted against the inverse of the pair separation. The laser will create pairs with the hole in the first excited state at pair separation R_1, and holes in the second excited state at separation R_2, and so on. The holes very quickly relax to their respective ground state, then recombine with the electrons, emitting light at $\hbar\omega = E_g - E_A - E_D + e^2/\varepsilon R$, where $E_A$is now the energy of the ground state of the hole with respect to the valence band. The energy difference between the laser and the emitted light is then the difference between the ground and excited state of the bound hole. This energy difference is characteristic of the particular acceptor,[2,6,11] and allows an accurate identification of the shallow acceptors present in the material.

The photon energy used for the experiment was chosen so that the ground state luminescence was near the peak of the donor-acceptor band. This procedure optimized the signal, since it pumped a part of the pair distribution for which there was both a large population of pairs and a high probability of recombination.

The formulas given above for the photon energy involved in the creation and recombination of a donor-acceptor pair assumed the pairs were separated sufficiently that the only important interaction energy between the donor and acceptor was a coulomb interaction between the ionized centers.

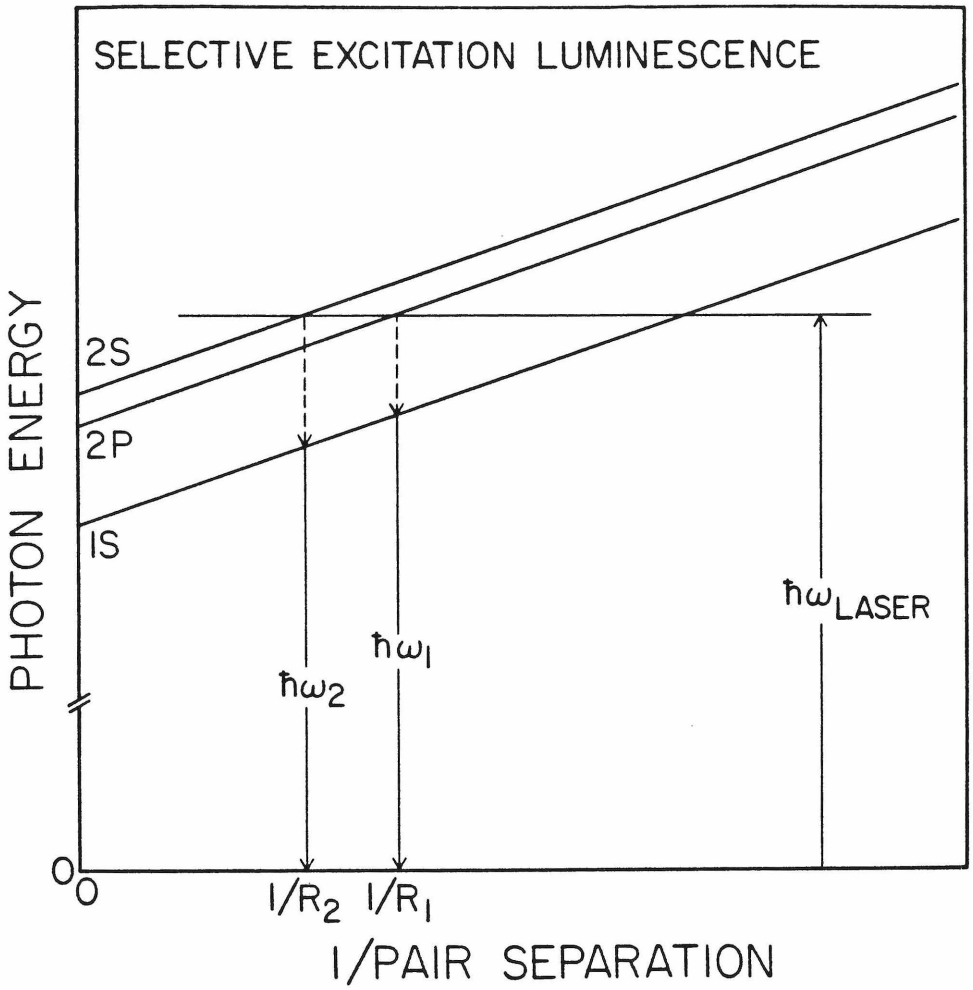

Figure 4.1: Schematic of the selective excitation luminescence process[2,3]. Energy required to create a donor-acceptor pair is plotted against the inverse to the pair seperation. The dye laser creates pairs with the hole in an excited state. The hole quickly relaxes to the 1S ground state, then radiatively recombines with the electron. The difference between the energy of the laser and that of the emitted light provides the ground state-excited state energy difference.

When the pairs are sufficiently close, other interactions become important, and the energies predicted above start to shift. However, it is possible to measure the amount of this shift experimentally. As will be shown below, for the pair separations of this experiment, the energy differences are accurately represented by the formulas given above.

4.2.2 Donor and acceptor states

The impurity levels in GaAs are well understood theoretically,[12,13] and have been investigated by other methods in high quality, epitaxial GaAs[1,6,11]. However, the identification of impurities in bulk grown material depends on making the correct correspondence between energy differences and energy levels. Therefore, the next few sections will review donor and acceptor levels as an aid to interpreting the results of the selective excitation luminescence experiment.

Shallow donors in GaAs are almost perfectly described[14,15] by the simple effective mass theory outlined in Chapter 1. The ground state binding energy of an electron on a donor is only 5.8 to 5.9 meV, depending on the donor.[14] The 2S and 2P excited states are bound with 1/4 of this energy,[14] and lie only 1.5 meV below the conduction band edge. As a consequence of the weak binding of the donor electrons, the spatial extent of the wavefunction is large. This will cause a broadening of the impurity levels for relatively small impurity concentrations due to overlap of wavefunctions.[2]

The acceptor states in GaAs have been very successfully described using an extension of effective mass theory that includes the degeneracy of the top of the valence band.[12,13] In this approach, first the spherical part of the effective mass equation, which includes the impurity potential, is solved.[12] The bound holes are labelled by a principal quantum number, the angular momentum of the envelope function, and a total angular momentum which comes from

coupling the angular momentum of the envelope function with the total angular momentum (J = 3/2) of the electronic state at the top of the valence band.[12] The cubic terms of the effective mass equation are then treated as a perturbation.[13]

Figure 4.2 shows the binding energy of the lowest acceptor states calculated in Ref. 13. The ground state has a 1S envelope function with a total angular momentum of 3/2. The last quantum number (Γ_8) describes the way the state transforms in the cubic crystal field. The first excited state has a P-like envelope function, with the first S-like excited state 0.4 meV above it. The next two excited states are both derived from a degenerate $2P_{5/2}$ state, which is split by the crystal field into a Γ_8 and Γ_7 state.

The theoretical binding energy is the same for all acceptors, since only the coulombic part of the impurity potential is included. However, since the core region is different for different impurities, the actual binding energy depends on which impurity is present.[2] The excited states are shifted in energy much less than the ground state. The first S-like excited state is shifted slightly,[2,6] because its wave function has an amplitude at the impurity core. However, the P-like excited states show almost no central cell shift.[11] This lack of shift of the excited states is very important, because it means that the ground to excited state energy difference is characteristic of the impurity.

4.3 EXPERIMENTAL

4.3.1 Apparatus

The equipment used for the selective excitation luminescence experiment will be described first. The Raman scattering experiment will be described, but only briefly, because it is almost identical to the selective excitation experiment.

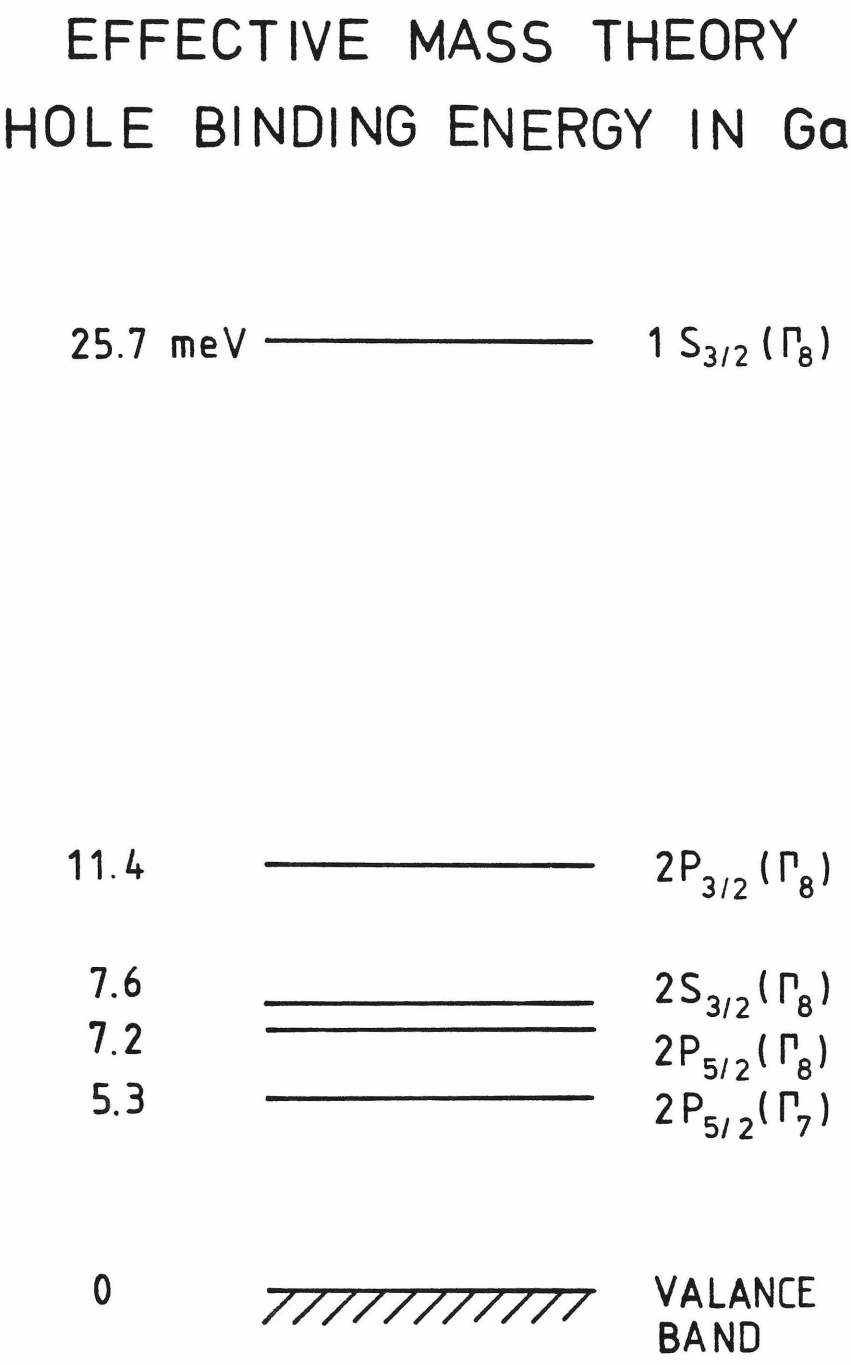

Figure 4.2: Calculated energy levels of a hole on an acceptor in GaAs in the effective mass approximation[12,13]. The energy of the level with respect to the valance band is given at the left. The label of the level is given at the right. The energies and the labels are those given in Ref. 13.

Finally, the luminescence equipment will be mentioned. Luminescence experiments in other materials are described in more detail in Chapters 2 and 3.

For the selective excitation luminescence experiment, a Coherent CR-3000K ion laser was used to pump a Coherent Model 590 dye laser. The dye was the carbo-cyanine dye DOTC, which could be tuned from ~760 nm to ~830 nm with a three plate birefringent filter inserted into the laser cavity (the filter had not been optimized for this wavelength range). This tuning element allowed line widths of between 0.1 and 0.2 meV. Energy resolution of better than 0.1 meV was obtained in most cases, as the lineshapes were symmetric Gaussians and their peaks could be determined with high accuracy.

The laser light was focused onto a sample which was immersed in liquid helium pumped below the lambda point in a Janis cryogenic dewar. The laser beam was incident on the sample at less than 45° from the normal to the surface. This was done to direct the specularly reflected beam away from the spectrometer aperture, which was at 90° from the laser light.

The emitted light was analyzed by scanning a Spex 1404 double grating spectrometer. The wavelength of the dye laser was measured by scanning across the laser wavelength with a neutral density filter in front of the spectrometer aperture. The luminescence signal was then recorded without the filter, scanning to longer wavelength from 5 to 10 Å past the laser wavelength. The gratings used were replica gratings, but ghost and background intensity proved to be insignificant at the wavelength differences of interest in this experiment. Luminescence background was not insignificant, but could be easily distinguished from the scattering processes we wished to observe. This was done by taking additional spectra with the pump laser at slightly different wavelengths. Those features selectively excited shifted in energy with the laser, while

background luminescence did not.

The signal was detected with an RCA C31034 photomultiplier tube. The photon pulses were then fed into a PAR 1120 amplifier discriminator, and counted by an ND60 multichannel analyzer.

The equipment for the Raman scattering was almost identical to that used for the selective excitation experiment except that the photon energy used was lower. Therefore a different carbo-cyanine dye (HITC) was used which could be tuned between 830 nm and 910 nm. A liquid-nitrogen-cooled S-1 response photomultiplier was used for these measurements. Aside from these changes the equipment and procedure for this experiment and the one described above were identical.

For the near band gap luminescence, a Spectra-Physics 155 He-Ne laser was used for excitation, and the C31034 photomultiplier tube was used for detection of the luminescence. For the deep luminescence, the Coherent Kr ion laser was used for excitation. The beam was mechanically chopped with a duty factor of 50%. The luminescence was detected with an SBRC InAs solid state detector, the output of which was fed into a PAR 124A lock-in amplifier. A signal from the chopper was used as a reference signal at the lock-in. The lock-in output was then fed into a voltage controlled oscillator, which produced pulses which were then counted with the multichannel analyzer. The spectrometer, dewar, and sample geometry were the same as in the other experiments.

4.3.2 Sample description

The GaAs samples were provided by the Hughes Research Laboratories, and we report sample descriptions which they furnished to us. Both samples studied were grown by the liquid encapsulated Czochralski method.[9] Sample 1 was

chrome doped, and is semi-insulating.[9] Sample 2 was not intentionally doped, and is p-type with $N_A - N_D \sim 10^{16}$ cm^{-3}.

4.4 RESULTS AND DISCUSSION

4.4.1 Luminescence

Figures 4.3 shows luminescence spectra for the two bulk-grown GaAs samples used in this study. In the upper spectrum, the signal to noise ratio is not large enough to resolve the bound exciton line. In the bottom spectrum, it can just barely be resolved on an expanded scale at 1512 meV. The two-hole transition of the bound exciton line cannot be resolved in either spectrum. In principle, the donor-acceptor pair luminescence bands centered at 1490 meV can be used to identify the acceptor involved in the transition.[2] However, this line has a rather high intrinsic width, as does the free- electron to bound-hole band seen at higher temperatures. It is difficult to differentiate between acceptors with ionization energies that differ by only a few meV, especially when the signal-to-noise is as poor as it is in the upper spectrum. Even with sufficiently good signal-to-noise, line shifts due to high impurity concentrations, which are possible in bulk-grown material, make identification by the position of the donor-acceptor band questionable.[2]

The low luminescence intensity from these shallow levels in the semi-insulating sample probably reflects a much higher deep level concentration, rather than a low shallow level concentration. This is indicated by the presence of a very high intensity deep luminescence band in the semi-insulating material. The band is very broad, and is centered at ~ 0.6 eV. This band has been seen in other bulk grown samples in luminescence spectra, and may be associated with chrome.[17,18] The band is at least 250 times less intense in the luminescence

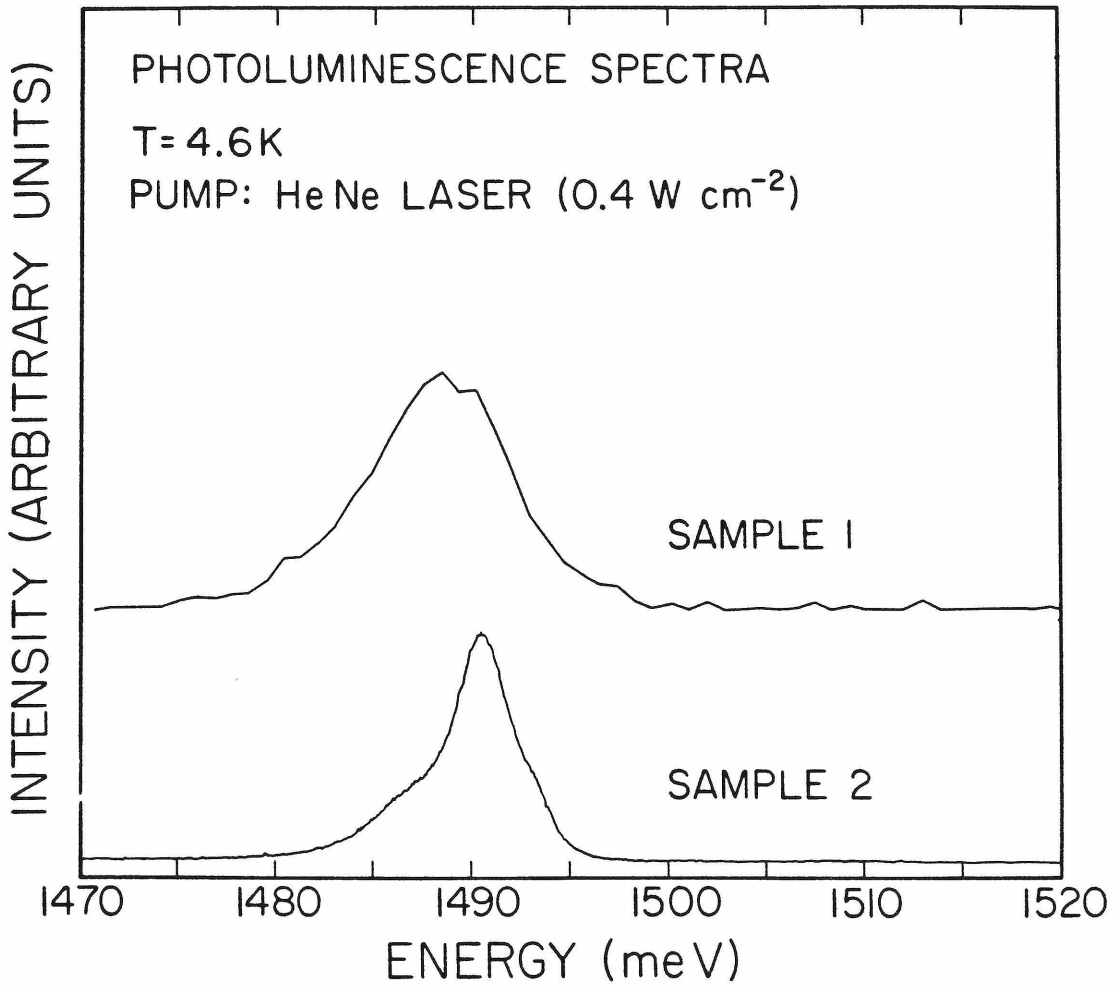

Figure 4.3: Photoluminescence spectra for two samples of bulk-grown GaAs, with above band-gap excitation. Intensity of emitted light is plotted on the vertical scale, against photon energy on the horizontal scale.

spectrum of the p-type sample.

4.4.2 Selective excitation luminescence

Selective excitation luminescence data provide an unambiguous identification of the acceptors. The three spectra in Fig. 4.4 are from sample 1, each taken with the dye laser at different photon energy. The spectra show intensity of luminescence plotted against energy difference between the laser and luminescence. This means the zero of energy in each case is the laser energy indicated above the spectrum at the right. Four peaks are apparent which stay at a fixed energy from the laser. The most intense peak is located 21.5 meV below the laser line, and is seen in all three spectra. Three other less intense peaks can be resolved, though not in all the spectra. They occur at 19.2, 21.5, and 25.0 meV. Interpreting the data as was done in Refs. 7 and 8, the principal line is assigned to the 1S - 2S energy difference, and the less intense lines are assigned to the 1S - 2P differences.

These results can now be compared to theoretical calculations,[13] and to measurements made on epitaxial GaAs by other methods. These earlier results, and the results of this study, are tabulated in Table 1. The two-hole shift measured for Zn doped epitaxial samples is 21.8 meV[2,6] and is very close to the 21.5 meV 1S - 2S difference measured for sample 1. The position of the less intense peaks line up well with the 1S - 2P differences measured using thermally activated photoconductivity[11] on epitaxial GaAs. Also included in the table, for reference, are the energy differences deduced from the effective mass calculation of Lipari and Baldereschi,[13], by replacing the calculated 1S position with that measured by Ashen, et al.[2] The matchup between our results and both theory and earlier results indicate the acceptor in this sample is Zn. It also demonstrates that selective excitation luminescence provides an unambiguous

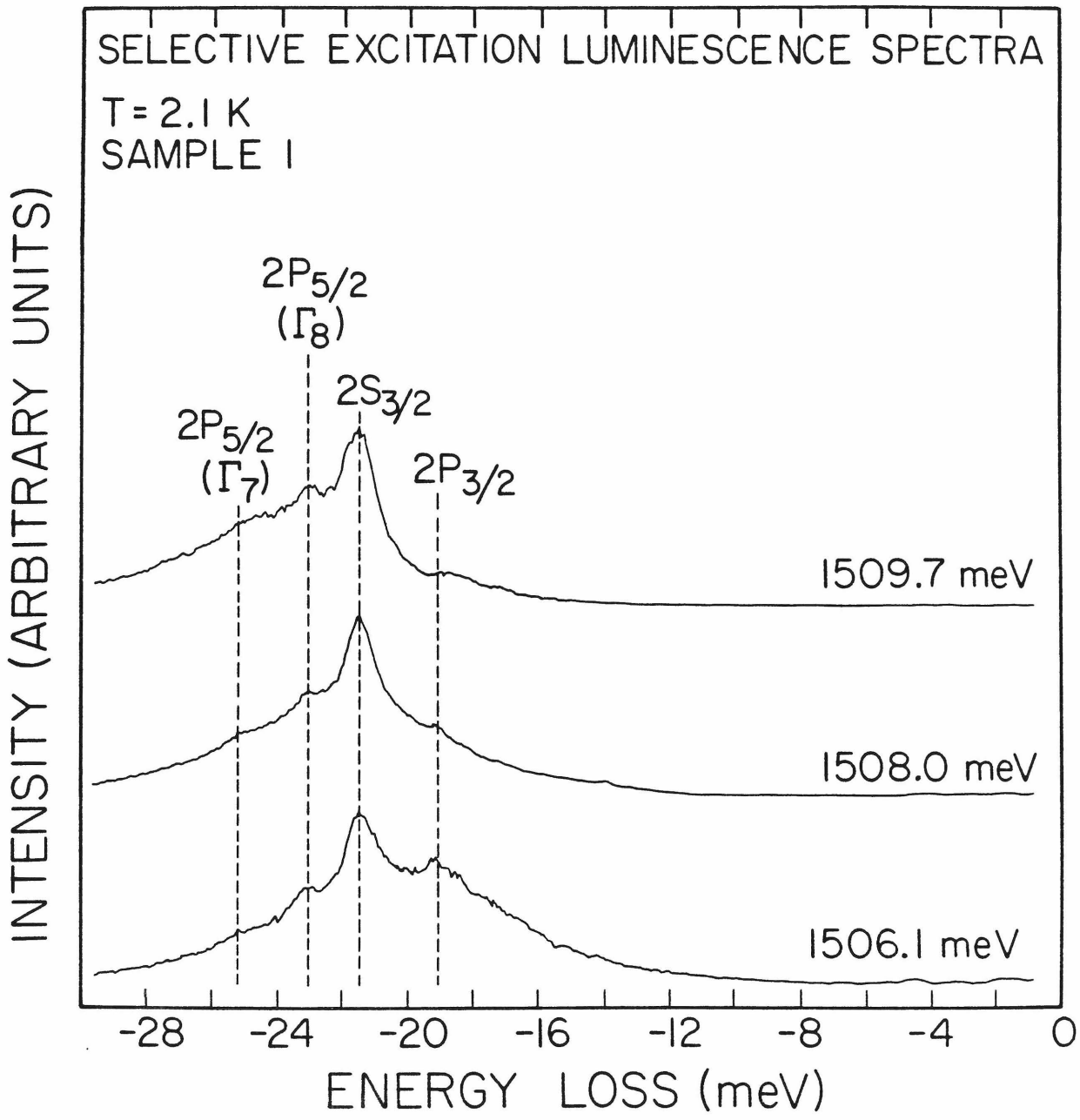

Figure 4.4: Selective excitation luminescence spectra for sample 1. Intensity of emitted light is plotted against the difference in photon energy of emitted light and that of the laser. Photon energy of the laser for each spectrum is given over the spectrum at the right.

Table I. Ground state to excited state splittings for the shallow acceptors C and Zn in GaAs, in meV. The labels for the acceptor levels are those used in Ref. 13.

		$1S_{3/2}$-$2P_{3/2}$	$1S_{3/2}$-$2S_{3/2}$	$1S_{3/2}$-$2P_{5/2}(\Gamma_8)$	$1S_{3/2}$-$2P_{5/2}(\Gamma_7)$
Zn	Theory [a]	19.3	23.1	23.5	25.4
	Photoconductivity [b]	19.4	...	23.2	25.0
	Two-hole shift [c]	...	21.8	...	...
	This study	19.2	21.5	23.1	25.0
C	Theory [a]	14.6	18.4	18.8	20.7
	Photoconductivity [b]	15.2	...	19.3	21.3
	Two-hole shift [c]	...	18.5	...	...
	This study [d]	15.2	18.5	19.3	21.4

a) Deduced from theoretical values quoted in Ref. 13 by replacing the calculated 1S position (25.7 meV)with that measured in Ref. 2: 26.0 meV for C and 30.7 meV for Zn.

b) Measured on epitaxial GaAs from Ref. 11.

c) Measured on epitaxial GaAs from Ref. 2.

d) Last two entries measured using Raman scattering.

method of determining the identity of shallow acceptors in bulk-grown GaAs.

We have also used this method to identify the acceptor in the second sample as carbon. Figure 4.5 shows four spectra taken on this sample, each at a different laser energy. Only two peaks are visible on these spectra, but they are sufficient to identify the acceptor. The principal line in this case is 18.5 meV below the laser energy (and is somewhat narrower than the principal line in sample 1). This is the two-hole shift measured for carbon doped epitaxial samples,[2,6] and identifies the dopant in our sample as carbon. The second line, at 15.2 meV, confirms the identification, because this is the 1S - $2P_{3/2}$ shift measured for carbon using photoconductivity.[11]. These results are also tabulated in Table 1.

Two points concerning line breadth and height could use further discussion. The increased line width in sample 1 could be indicative of much higher impurity concentration. The presence of a third impurity near the pair involved in the transition would perturb the energy levels of the hole. Since the excited state energy would not, in general, be shifted by the same amount as the ground state, this would lead to a broadening of the lines we observe. This perturbation of the hole levels brings up the second point, which is why the 1S - 2P transitions are more intense in sample 1. Since the hole must undergo what is apparently a parity forbidden relaxation process[7] to reach the ground state from a P-like excited state, a perturbation of the wavefunction that lowered its symmetry could enhance the relaxation. Therefore, both the breadth of the lines and the increased intensity of the 1S - 2P lines in sample 1 could be explained by a much higher impurity concentration in this sample than in sample 2.

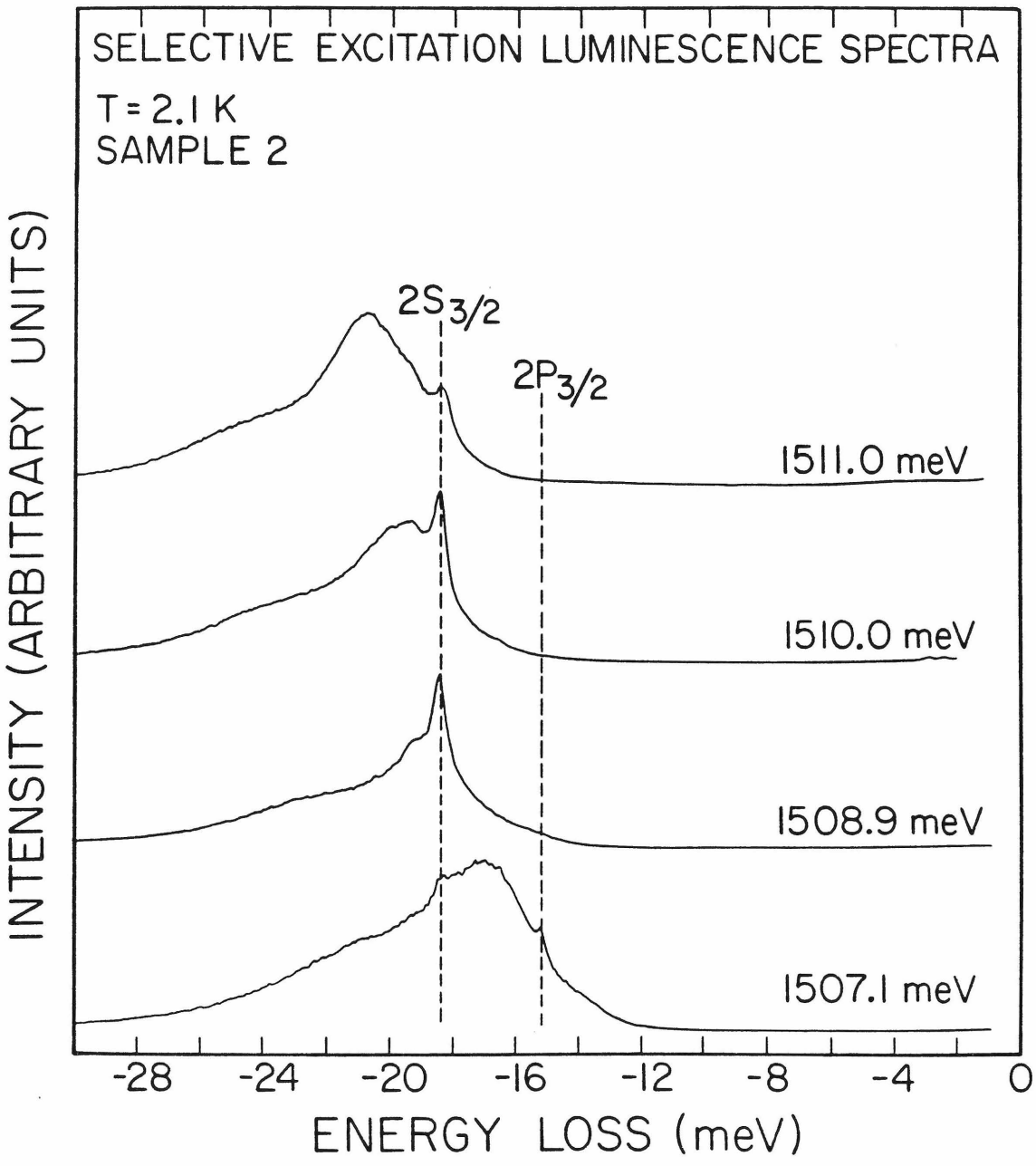

Figure 4.5: Selective excitation luminescence spectra for sample 2. Intensity of emitted light is plotted against the difference in photon energy of emitted light and that of the laser. Photon energy of the laser for each spectrum is given over the spectrum at the right.

4.4.3 Raman scattering

For the p-type sample, Raman scattering could also be used to measure the ground to excited state energy differences. Figure 4.6 shows two energy loss spectra from sample 2. These spectra were taken with the dye laser photon energy too low to create donor-acceptor pairs. A second order scattering process leaves the acceptors in an excited state, so the energy loss is the ground state to excited state energy differences. Four lines are visible in these spectra. The most intense line is again assigned to the 1S to 2S energy difference, while the other three lines provide the 1S to 2P energy differences. The line due to the lowest two states, at 15.1 and 18.5 meV, agree with the energy differences measured in selective excitation luminescence. The additional two lines, at 19.3 meV and 21.4 meV, are at the energy differences measured for the $2P_{5/2}$ states for C in epitaxial samples. This confirms the identification of the impurity in sample 2 as carbon. No Raman signal could be detected from sample 1. This absence of signal is expected as the acceptors are not occupied by holes in semi-insulating material.

Beside confirming the identity of the acceptor in sample 2 as carbon, the Raman scattering data provide another very useful piece of information. For very close donor-acceptor pairs, the acceptor wavefunction is sufficiently perturbed to change the energy of the states. This would lead to a shifting of the ground state to excited state energies measured in this experiment, since in general the excited states would shift in energy more than the ground state. However, for the separations of the donor-acceptor pairs excited in this experiment, this shifting of the energy levels is estimated to be very small. First, as the laser energy is changed, which would change the separation of the excited pair, the energy difference measured does not shift. In addition, the Raman

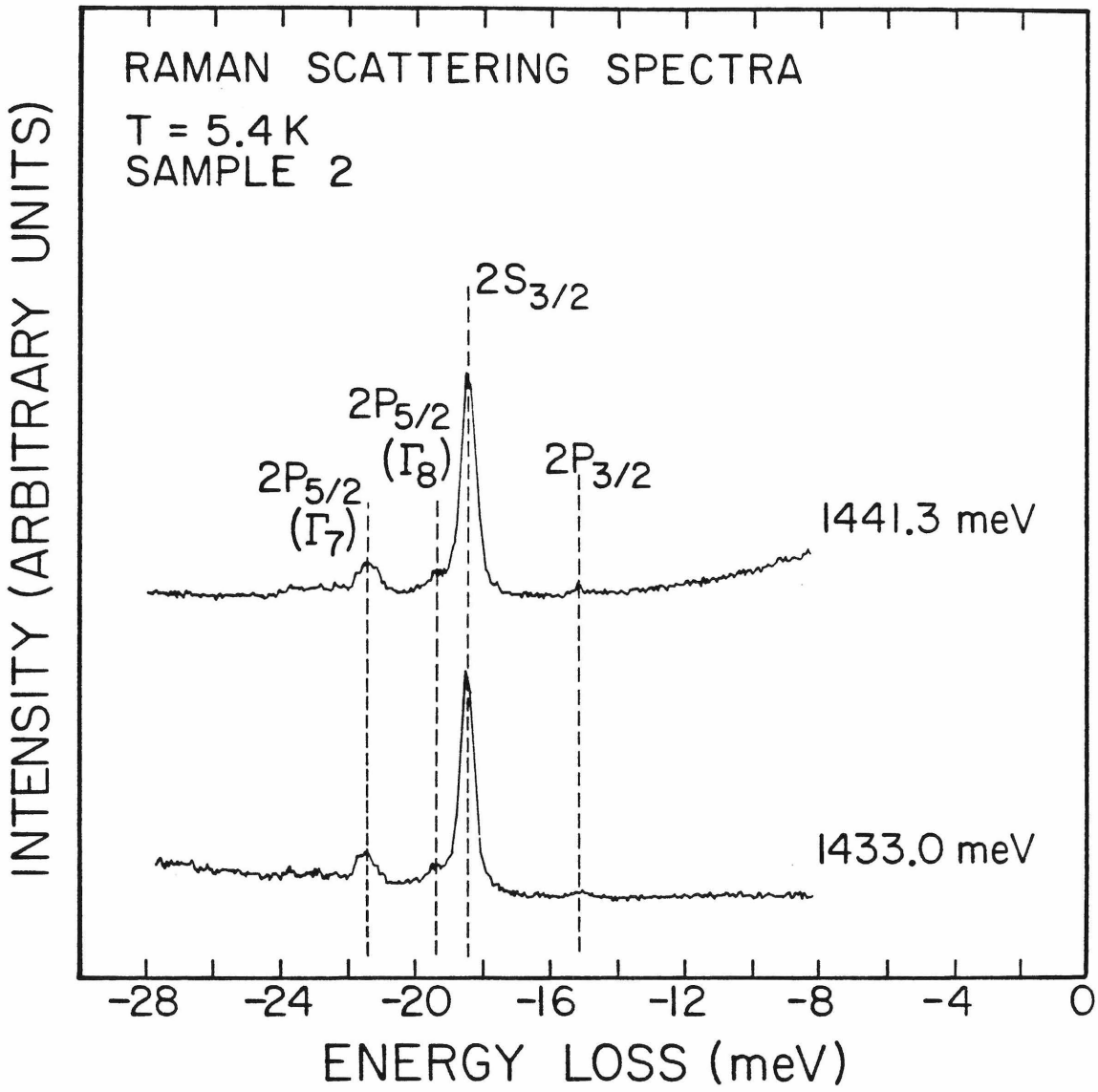

Figure 4.6: Raman scattering spectra for sample 2. Intensity of emitted light is plotted against the difference in photon energy of emitted light and that of the laser. Photon energy of the laser for each spectrum is given over the spectrum at the right.

scattering data gives the energy separations for isolated acceptors, and these energies match those measured with selective excitation luminescence to within the experimental uncertainty of the measurements.

4.4.4 Absence of donor levels

The complete absence of donor levels in the analysis of these lines should be discussed. The first excited state of the donor is only ~ 1.5 meV[14] below the conduction band minima, and these weakly bound states may be thermally ionized with high probability. However, even if the electrons do not thermalize, it may not be possible to resolve recombination from those pairs with the electron created in an excited state. The very extended excited donor level may be substantially broadened by interaction with other impurities. This could lead to a line breadth which is too wide to resolve against the background luminescence. The highest lying acceptor state observed is still ~ 6 meV below its ionization threshold, and would show much less of this broadening since its spatial extent would be correspondingly less.

4.4 SUMMARY

In conclusion, we have measured the excited state levels of shallow acceptors in bulk-grown GaAs, using selective excitation luminescence. The principal shallow acceptor was identified as Zn in the semi-insulating sample 1, and C in the p-type sample 2. The near band-edge luminescence in sample 1 was very weak, due to a large concentration of deep levels. This, and the high overall concentration of impurities probably present in the sample, made identification of the shallow impurity by straightforward luminescence difficult. The energy level differences in sample 2 were also measured by the use of Raman scattering. This demonstrated that the energy differences measured in the selective excitation luminescence experiment were the energy level differences of the isolated

acceptor, and confirmed the identity of the acceptor in this sample as C.

While these levels have been measured in GaAs before, it was done using different methods in high quality, epitaxial layers. This is the first time the levels have been measured in bulk-grown GaAs, where the other methods are not as useful. In doing so, selective excitation luminescence has been shown to be a valuable tool in identifying the shallow acceptors in bulk-grown GaAs.

REFERENCES

1. H. J. Queisser, Appl. Phys. **10**, 275 (1976).

2. D. J. Ashen, P. J. Dean, D. T. J. Hurle, J. B. Mullin, A. M. White, and P. D. Greene, J. Phys. Chem. Solids **36**, 1041 (1975).

3. G. S. Mitchard, and T. C. McGill, Appl. Phys. Lett. **37**, 959 (1980).

4. G. M. Martin, in Semi-Insulating III-IV Conference Proceedings, University of Nottingham, April (1980).

5. W. Schairer, T. O. Yep, Solid State Commun. **9**, 421 (1971).

6. A. M. White, P. J. Dean, D. J. Ashen, J. B. Mullin, M. Webb, B. Day, and P. D. Greene, J. Phys. C **6**, L243 (1973).

7. P. J. Dean, D. J. Robbins, and S. G. Bishop, Solid State Commun. **32**, 379 (1979).

8. P. J. Dean, D. J. Robbins, and S. G. Bishop, J. Phys. C **12**, 5567 (1979).

9. H. Tews, and H. Venghaus, Solid State Commun. **30**, 219 (1979).

10. H. Tews, H. Venghaus, and P. J. Dean, Phys. Rev. B **19**, 5178 (1979).

11. R. F. Kirkman, R. A. Stradling, and P. J. Lin-Chung, J. Phys. C **11**, 719 (1978).

12. A. Baldereschi, and N. O. Lipari, Phys. Rev. B **6**, 2697 (1973).

13. A. Baldereschi, and N. O. Lipari, Phys. Rev. B **9**, 1525 (1974).

14. G. E. Stillman, D. M. Larsen, C. M. Wolfe, R. C. Brandt, Solid State Commun. **9**, 2245 (1971).

15. M. S. Skolnick, A. C. Carter, Y. Couder, and R. A. Stradling, J. Opt. Soc. Am. **67**, 947 (1977).

16. H. V. Winston, private communication.

17. W. H. Koshel, S. G. Bishop, and B. D. McCombe, Solid State Commun. **19**, 521 (1976).

18. B. Deveaud, and P. N. Favennec, Solid State Commun. **24**, 473 (1977).